KIF13A MEDIATES INFLUENZA A VIRUS RIBONUCLEOPROTEINS TRAFFICKING

Ana Ramos-Nascimento[1,2], Bárbara Kellen[3], Filipe Ferreira[1], Marta Alenquer[1], Silvia Vale-Costa[1], Graça Raposo[4], Cédric Delevoye[4] and Maria João Amorim[1,*]

[1] Cell Biology of Viral Infection Lab, Instituto Gulbenkian de Ciência, Oeiras, Portugal
[2] Institute of Virology, Hannover Medical School, Hannover, Germany
[3] Science4U, MARL Espaços CC02 e CC03, São Julião do Tojal, 2660-421, Loures, Portugal
[4] Institut Curie, PSL Research University, CNRS, UMR144, Structure and Membrane Compartments, 75005 Paris, France
*Corresponding author

Tel: + 351 214407905

Fax: + 351 214407970

Email mjamorim@igc.gulbenkian.pt

Classification: Host-Microbial Interactions, Eukaryotic cells; Molecular and Cellular Biology

JCS Advance Online Article. Posted on 23 October 2017

ABSTRACT:

Influenza A is a rapid evolving virus, successful in provoking periodic epidemics and occasional pandemics in humans. Viral assembly is complex as the virus incorporates an eight-partite segmented genome of RNA (in the form of viral ribonucleoproteins, vRNPs). Genome assembly, with implications to public health, is not completely understood. It was reported that vRNPs are transported to the cell surface on Rab11 vesicles using microtubules, but no molecular motor has been assigned to the process. Here, we have identified KIF13A, a member of the kinesin-3 family, as the first molecular motor efficiently transporting vRNP-Rab11 vesicles during IAV infection. Depletion of KIF13A resulted in reduced viral titres and less accumulation of vRNPs at the cell surface, without interfering with the levels of other viral proteins at sites of viral assembly. In addition, in overexpression conditions and using two artificial methods able to displace vRNP-Rab11 vesicles, KIF13A augmented vRNP levels at the plasma membrane. Together our results show that KIF13A is an important host factor promoting influenza A vRNP transport, which is a crucial step for viral assembly.

SUMMARY STATEMENT:

Progeny RNA from influenza A virus is transported to the cell surface on vesicles of the recycling endosome to be packaged into assembling virions. Here, we have identified the first molecular motor, KIF13A, able to carry these vesicles and positively influence the localization of vRNPs at the cell surface and viral assembly.

INTRODUCTION:

Influenza A virus (IAV) genome is single-stranded of negative-sense RNA and segmented, divided into eight independent replication units. Each unit is composed of identical RNA termini, and the 3' and 5' are partially complementary and form a dsRNA region that accommodates the viral heterotrimeric RNA dependent RNA polymerase (RdRp) (Pflug et al., 2014). The remainder RNA contains distinct coding regions, of variable sizes coated by nucleoprotein (NP) molecules which are placed every 24 nucleotides on average (Arranz et al., 2012). In the virion, the eight distinct viral ribonucleoproteins (vRNPs) occupy the inner core and are spatially distributed with seven segments surrounding a central one in a "7+1" arrangement (Noda and Kawaoka, 2010). Of the up to 18 identified proteins encoded by the virus (Yamayoshi et al., 2015), only 5 additional viral factors to those forming vRNPs are essential structural components of the virion. The viral nuclear export protein (NEP) is found attached to vRNPs in modest amounts. Surrounding the genomic core is a layer of the matrix protein 1 (M1), that is coated by a host derived membrane containing 3 antigenic viral transmembrane proteins: hemagglutinin (HA), neuraminidase (NA) and matrix protein 2 (M2) (Hutchinson et al., 2014, Shaw et al., 2008).

The mechanisms underlying virion formation inside the host cell are not fully understood. Viral assembly comprises the formation of the supra-molecular complex described above at the cell surface, and propels viral budding and release. Viral genome complex formation has been reported to be fully dependent on the establishment of RNA-RNA interactions between the different vRNPs (as reviewed in (Gerber et al., 2014, Giese et al., 2016, Hutchinson et al., 2010)). However, IAV assembly is heavily dependent on host processes, namely for transporting components to the budzone. The transport of the viral transmembrane proteins, HA, NA and M2 to the plasma membrane occurs via the secretory pathway (Doms et al., 1993) and involves the coat protein I (Sun et al., 2013). M1 might be transported along with vRNPs (Noton et al., 2007), M2 (Chen et al., 2008) and/or lipids to the surface, but a detailed analysis of the transport of the

M1 pool included in virions is still missing. In the case of vRNPs, the eight-distinct segments are synthesized in the host cell nucleus as independent entities, exported to the cytoplasm (Elton et al., 2001, Ma et al., 2001) and transported to the surface. The endocytic recycling compartment (ERC) was shown to be required for this transport, with vRNPs binding to the major coordinator of ERC trafficking, the GTPase Rab11 (Amorim et al., 2011, Avilov et al., 2012, Eisfeld et al., 2011, Momose et al., 2011). In the healthy cell, Rab11 is switched off or on by binding to GDP or GTP, respectively (Xiong et al., 2012). Activated Rab11 acquires sequential affinity for a series of molecular motors, membrane tethers and v-SNARES, responsible for vesicular movement along cytoskeletal tracks, attachment to and fusion with membranes, respectively (Welz et al., 2014). In relation to molecular motors, Rab11 vesicles were reported to associate with: myosin Vb, dynein light chain 1 and 2, KIF5a and KIF3 of the kinesin-1 and -2 families, respectively ((Fan et al., 2004, Lapierre et al., 2001, Provance et al., 2008, Roland et al., 2011, Schonteich et al., 2008, Perez Bay et al., 2013) and reviewed in (Vale-Costa and Amorim, 2016b)). Interestingly, these motors require adaptors for Rab11 binding, and these adaptors belong to a vast family collectively called Rab11-interacting-proteins (FIPs) (Horgan and McCaffrey, 2009). Recently, Rab11 vesicles were shown to associate with an additional motor, KIF13A, from the kinesin-3 family, without recurring to FIPs for binding (Delevoye et al., 2014). In infection, IAV modulates Rab11 trafficking and, as a consequence, this dynamic chain of events is altered. Known effectors of Rab11 are prevented from binding to Rab11 (Vale-Costa et al., 2016), transferrin recycling is reduced (Kawaguchi et al., 2015, Vale-Costa et al., 2016), and FIPs that are essential components of the pathway were found to be dispensable for IAV infection (Bruce et al., 2010, Momose et al., 2011). Mechanistically, vRNPs were found to out-compete FIPs for Rab11 binding (Vale-Costa et al., 2016). Therefore, although several papers have confirmed the importance of Rab11 for vRNP delivery to the surface (Amorim et al., 2011, Avilov et al., 2012, Eisfeld et al., 2011, Momose et al., 2011) and viral assembly (Chou et al., 2013, Lakdawala et al., 2014), it is unclear which host factors are involved in transporting

vRNPs to sites of viral assembly. In particular, no molecular motor was identified as being able to transport vRNP-Rab11 vesicles, and it is unknown if vesicular movement on microtubules is modified by the virus. On the one hand, vRNPs were shown to transit with directed and intermittent movements, with speeds compatible with using microtubule and actin (Amorim et al., 2011, Avilov et al., 2012). Consistent with the usage of the cytoskeleton, NP was shown to co-localise with actin (Avalos et al., 1997, Digard et al., 1999, Roberts and Compans, 1998, Simpson-Holley et al., 2002), and pharmacological destabilization of the microtubule network disrupted shuttling of vRNPs to the plasma membrane (Amorim et al., 2011). On the other hand, drugs acting on actin or microtubule integrity have mild effects in viral production (Amorim et al., 2011, Momose et al., 2007, Simpson-Holley et al., 2002), despite impacting dramatically in virion morphology (Roberts and Compans, 1998, Simpson-Holley et al., 2002). Furthermore, as vRNP binding to Rab11-GTP out-competed the binding of FIPs, it is possible that the vesicular flow is compromised upon infection (Momose et al., 2011, Vale-Costa et al., 2016). In agreement, it was shown that vRNPs associate with Rab11a at ~300 nm from the nucleus but disassociate at ~500 nm from the cell surface (Nturibi et al., 2017), which indicates that Rab11 might not be the final factor delivering vRNPs to the plasma membrane (Eisfeld et al., 2015, Vale-Costa and Amorim, 2016a).

Here, we report that KIF13A positively modulates IAV infection, affecting the trafficking and peripheral localization of vRNPs, but not of the viral transmembrane proteins HA and M2. Depletion of KIF13A did not disturb the initial steps of viral infection, including viral entry, replication and gene expression. Our results suggest a model in which vRNP transport is facilitated by KIF13A on Rab11 vesicles and not by molecular motors that require FIPs for association to Rab11.

RESULTS:

KIF13A depletion reduces viral production

To answer whether KIF13A is necessary for IAV infection, we depleted cells of this molecular motor with specific siRNAs (Fig 1A-B, S1), infected or mock-infected cells with influenza A/Puerto Rico/8/34 (PR8) and quantified viral production. KIF13A-depleted cells resulted in over 10 and 5-fold reduction in viral titers relative to cells treated with non-targeting siRNAs (siNT) at 6 and 10h p.i., respectively, showing that KIF13A is required for the virus life-cycle (Fig 1A). When KIF13A mRNA levels were quantified, a consistent average depletion of 80% in mock-infected cells was obtained. In infected cells, depletion was not as efficient averaging 70%, and 60% reduction at 6 and 10h p.i.. Interestingly, infection specifically targets KIF13A for depletion, especially late in infection, as cells treated with non-targeting siRNAs consistently exhibited a drop of roughly 60% at 10h p.i. (Fig 1B). The significance of this has not been explored further but suggests a viral induced restriction in KIF13A amounts. Endogenous levels of KIF13A protein were just above the detection limit and depletion was difficult to quantify (Fig S1A). Western blot analysis showed no detectable differences in viral gene expression (Fig 1C,D) between the two siRNA treated samples in the times analysed. Our results suggest that KIF13A does not affect the initial steps of viral infection, since viral protein expression is similar in cells with and without KIF13A. To evaluate knock-down levels of KIF13A protein, we transfected GFP or GFP-KIF13A-WT or a siRNA-resistant GFP-KIF13A form, treated cells with specific RNAs concomitantly, observing that KIF13A depletion at the protein level was very efficient (Fig S1B).

Our results indicate that KIF13A is required for IAV lifecycle, at a step downstream of vRNP nuclear import and viral mRNA synthesis.

KIF13A depletion influences vRNP transport but not that of HA and M2

Given that KIF13A was shown to bind and transport Rab11 vesicles (Delevoye et al., 2014), and vRNPs were shown to use Rab11 vesicles for reaching sites of assembly (Amorim et al., 2011, Avilov et al., 2012, Eisfeld et al., 2011, Momose et al., 2011), we sought to observe the effect of KIF13A-depletion in vRNP localization during the course of infection. It is well-established that at early time points, vRNPs accumulate in the nucleus (where they are synthesized) and from 6h onwards localise mainly in the cytoplasm. Cytosolic vRNPs start by accumulating at the microtubule organizing center and then become disperse throughout the cytosol, co-localising with the host protein Rab11 in puncta that enlarge over time (Amorim et al., 2011). Enlarged puncta were shown to correspond to clustered vesicles that result from impaired vesicular flow (Vale-Costa et al., 2016, Vale-Costa and Amorim, 2016a). The nuclear/cytoplasmic time-dependent changes in vRNP localization as assessed by NP staining (Fig 2A,B) and Pearson correlation values (Fig 2C) between vRNPs and Rab11 were not statistically different in cells treated with KIF13A and non-targeting siRNAs. This indicates that in the absence of KIF13A, vRNPs still co-localise with Rab11, suggesting that the lack of this molecular motor does not interfere with loading of progeny RNA into recycling membranes. However, the accumulation of vRNPs at the periphery was significantly lower in KIF13A-depleted cells (Fig 2E). Thus, we concluded that depletion of KIF13A is required for the peripheral positioning of vRNPs. Interestingly, the progressive enlargement in Rab11 and vRNPs cytoplasmic areas previously reported (Amorim et al., 2011, Chou et al., 2013, Eisfeld et al., 2011, Lakdawala et al., 2014, Vale-Costa et al., 2016) was reduced relative to the control (Fig 2D), suggesting either a decrease in vesicular biogenesis or movement (Delevoye et al., 2014) in the absence of KIF13A.

We also asked whether KIF13A interfered with the levels of the viral transmembrane proteins HA and M2 that are delivered to the surface by a membrane trafficking pathway

independent of Rab11 (Doms et al., 1993). Cells were treated with control and KIF13A specific siRNAs, and challenged with PR8. At 10h p.i. the surface levels of HA and M2 were measured by flow cytometry. KIF13A-depleted cells presented higher amounts (~150% and ~130%, respectively) of these two viral proteins at the surface when compared to control cells (Fig 2F). As previously proposed (Amorim et al., 2013), this result suggests that HA and M2 proteins are transported to the cell surface normally, but are not released because of reduced viral egress.

Our data strongly indicate that KIF13A influences the low of vRNPs on Rab11 vesicles without interfering with the trafficking of other viral transmembrane proteins.

KIF13A overexpression biases vRNP distribution to the periphery

Our data indicates that KIF13A impacts on vRNP cytoplasmic distribution. To strengthen this observation, cells were transfected with GFP as control, or with either a GFP tagged full-length KIF13A (GFP-KIF13A-WT, henceforward KIF13A-WT) or a truncated form able to attach vesicles but not microtubules (GFP-KIF13A-ST, henceforward KIF13A-ST) that was described in (Delevoye et al., 2014) and here in Fig 3D. Cells were subsequently infected or mock infected with PR8, and NP distribution assessed during infection. In mock infected cells, the three proteins distributed as described before (Delevoye et al., 2014). GFP dispersed throughout the cytosol (Figs 3A, S2A, S3). KIF13A-WT, was found in the cytosol (in tubules and puncta), accumulating in peripheral spots (Fig 3B, S2B, S3B), partially co-localising with Rab11 (Fig 3B). KIF13A-ST localized to cytosolic puncta also occupied by Rab11 (Fig 3C, S2C, S3C). In infected cells transfected with GFP, NP displayed similar time-dependent changes in localization to those described above (Amorim et al., 2011, Amorim et al., 2013, Vale-Costa and Amorim, 2016a): early nuclear accumulation, followed by cytoplasmic display from 6h onwards. The cytoplasmic phase of vRNPs included the initial accumulation of vRNA in discrete puncta (and perinuclar accumulation) and at later time points, the discrete puncta were replaced by larger structures dispersed throughout the cytoplasm (Figs 3A, S2A, S4A). The overexpression

of KIF13A-WT resulted in extensive tubulation of the membrane associated with vRNPs, in close proximity to KIF13A tracks (Fig 3B). Further, it led to the accumulation of vRNPs at the periphery in areas containing Rab11 agglomerates and KIF13A (Figs 3B, S2B, S4B (untreated).To understand whether KIF13A-dependent vRNP peripheral localization required its motor activity, the distribution of NP was assessed in cells expressing KIF13A-ST. Strikingly, NP localization was similar to that observed in the GFP control, and at 8 and 10h p.i. KIF13A-ST was found juxtaposed (partially co-localising with) vRNP-Rab11 enlarged puncta (Fig 3C, S2C, S2D, S4C (untreated)). To measure the vRNP peripheral accumulation in the different conditions over the course of infection, we applied the same method as in Fig 2E. NP peripheral localization (relatively to the whole cell) in cells challenged with PR8 and transfected with either GFP or KIF13A-ST did not differ during the course of infection. However, NP peripheral localization in cells transfected with KIF13A-WT was significantly higher than the other conditions at the times tested. Our results, therefore, show that KIF13A can influence the distribution of vRNP-containing-Rab11 vesicles using its motor activity.

KIF13A was shown to interact with the three isoforms of Rab11 (Rab11a, Rab11b and Rab25) by yeast two hybrid systems and pull down assays (Nakagawa et al., 2000, Delevoye et al., 2009, Delevoye et al., 2014). Rab11a and Rab11b are highly homologous and are both implicated in IAV infection (Bruce et al., 2010). Attempts to observe a complex between vRNP-Rab11-KIF13A at endogenous levels failed. In cells overexpressing GFP or KIF13A-WT or KIF13A-ST and cherry-Rab11a WT or cherry-Rab11b WT, Rab11a and Rab11b were selectively pulled down with both forms of KIF13A in mock and infected cells at very low, but similar levels (Fig 4). This result suggests that infection does not change this interaction, conversely to what was described for FIPs (Vale-Costa et al., 2016). However, the low levels of Rab11a/b selectively purified with KIF13A were insufficient to specifically pull down vRNPs (Fig 4), and whether vRNPs form a tripartite complex together with Rab11 and KIF13A remain to be explored.

vRNP agglomeration induced by the drug nucleozin is affected by KIF13A overexpression

Given that we found no biochemical association between KIF13A-Rab11-vRNPs, we sought to confirm if KIF13A impacts the vRNP distribution in IAV infected cells using several additional complementary strategies. First, we used the drug nucleozin (Kao et al., 2010), previously demonstrated to permanently bind colliding vRNP-Rab11-vesicles when added at late time points (Amorim et al., 2013). Briefly, the drug was shown to have affinity for several domains on NP (the viral protein coating vRNPs) (Kao et al., 2010), and hence, when vesicles (carrying vRNPs on the outside) collide, they attach to each other. As time progresses, nucleozin induced vRNP-Rab11-vesicular agglomerates increase in size, producing dramatic structures that collapse near the microtubule organizing center (minus-end) (for detailed description on nucleozin readers are referred to (Kao et al., 2010, Amorim et al., 2013)). Of note, as nucleozin has affinity for NP and not Rab11, its action is specific to infected cells ((compare treated/untreated samples in Figs S3, S4) and (Amorim et al., 2013)). Conversely to the nucleozin induced movement of vRNPs to the perinuclear region, KIF13A transports Rab11 vesicles towards the plus-end (or the cell surface) (Delevoye et al., 2014). Hence, we reasoned that KIF13A would counteract the action of nucleozin by applying a force in the opposite direction that would either alter a) the shape of agglomerated vesicles or b) the time agglomerates take to collapse at the perinuclear region (Fig 5C).

Consistent with exerting opposing forces, nucleozin treated cells overexpressing KIF13A-WT originated vRNP-agglomerates more distant from the nucleus than those observed in cells expressing GFP (as control) or KIF13A-ST (without motor capacity) (Fig 5A). For an unbiased and accurate quantification of nucleozin induced perinuclear accumulation of vRNPs/Rab11, we generated an automated tool to evaluate the amount of vRNPs/Rab11 within 2 μm from the nucleus (Fig 5B). Both NP and Rab11 staining were significantly less intense close to the nucleus in cells overexpressing KIF13A-WT treated with nucleozin when compared to those in

cells with GFP or KIF13A-ST, indicating that KIF13A operates as a force able to counteract nucleozin action (Fig 5B).

Nucleozin induced vRNP-agglomerates were shown to include Rab11 ((Amorim et al., 2013) and Fig 5D (right)) but exclude a series of organelle markers (Golgi, endoplasmic reticulum, lysosomes). We reasoned that given that the candidate proteins exhibit similar dynamics of colocalization with the vRNPs and are specifically trapped in nucleozin-induced vRNP aggregates, this strongly suggests that they form functional complexes with the vRNPs (Amorim et al., 2013). To understand if this was the case for KIF13A, we quantified Pearson correlation values of GFP, KIF13A-WT, KIF13A-ST with vRNPs and Rab11. GFP and KIF13A-WT were found not to co-localise with vRNPs or Rab11 in infected cells, regardless of nucleozin. However, as just demonstrated, KIF13A-WT counteracts nucleozin induced aggregate formation by exerting a force in the opposite direction, and with GFP fused to the motor part, proximity between all components could be hard to evaluate in this system. Hence, we reasoned that KIF13A-ST would be a better choice for this measurement, as it is devoid of the pulling capacity. In agreement, in the presence of nucleozin, KIF13A-ST co-localised with both vRNPs and Rab11, consistent with being in close proximity (Fig 5D). Together, our results suggest that KIF13A not only influences the location of vRNPs and Rab11 in infected cells, but might also be part of a complex with these vesicles.

KIF13A biases mitoRab11-vRNP distribution to the surface

As a second additional strategy to understand if KIF13A transports vRNPs on Rab11 vesicles and as a way to discriminate if it binds to either Rab11a and Rab11b, we used an artificial targeting system to anchor Rab11a and Rab11b to the mitochondria (by fusing Rab11a/b constitutively active (CA) with the mitochondrial targeting sequence (MTS) of Tom20 (henceforward mitoRab11a/b)) and analyse relocation of individual effectors (Fig 6B). This

strategy has been successfully used by us to show that FIPs competed with vRNPs for Rab11a binding (Vale-Costa et al., 2016). MitoRab11aCA but not mitocherry control recruited FIPs to the mitochondria ((Vale-Costa et al., 2016) and Fig S5A). When vRNPs and FIPs were co-expressed, a decrease in vRNP localization to the mitochondria was observed (Vale-Costa et al., 2016). We applied the same protocol here and transfected mitocherry or mitoRab11a/b and GFP or KIF13A-WT or KIF13A-ST to mock and infected cells. In mock or infected cells, GFP and KIF13A-WT did not relocalize to the mitochondria (Fig 6, S5B,C, S6). However, KIF13A-ST, in the presence of mitoRab11a, but not mitocherry, was found juxtaposed to this organelle (Fig6, S5B,C, S6), indicating that, if not part of the complex, this motor (when not exerting pulling forces) is found in close proximity to mitoRab11a. In infection, vRNPs redistributed to the mitochondria in an undifferentiated manner regardless of KIF13A (Fig S5 and 6A-C). Furthermore, overexpression of KIF13A-WT biased the distribution of mitoRab11a (Figs 6A,C, S5B,C middle panels, S6) and of vRNPs to places at the cell surface displaying KIF13A-WT (Figs 6, S5C). Similar observations were acquired for mitoRab11b. Quantification of peripheral localization of mitoRab11a or mitoRab11b, and of vRNPs was done by measuring the percentage of these components within 3μm of the plasma membrane relative to the whole cell (3μm were chosen given the large size of mitochondria). In the presence of KIF13A-WT, mitoRab11a/b and vRNPs were found significantly closer to the periphery than the control GFP, confirming the results obtained. In addition, this biased localization was, at least for mitoRab11b and vRNPs dependent of the motor activity of KIF13A, as the -ST form failed to do so with the same extent (Figs 6C,D, S5,6).

DISCUSSION:

It was shown that vRNPs are transported to the cell periphery using the recycling pathway (via Rab11) at speeds compatible with movement along microtubules (Amorim et al., 2011, Avilov et al., 2012, Eisfeld et al., 2011, Momose et al., 2011). In addition, it is well established that IAV not only uses the recycling pathway but alters it, as demonstrated by Rab11 redistribution during infection, changing from distinct puncta to enlarged structures (Lakdawala et al., 2014, Chou et al., 2013, Amorim et al., 2011, Avilov et al., 2012, Eisfeld et al., 2011). Mechanistically, Rab11 alterations were reported to be, at least partially, a consequence of a viral-induced halt in recycling endosome functioning (Vale-Costa et al., 2016, Vale-Costa and Amorim, 2016a). Several lines of evidence support this hypothesis including reduction in transferrin recycling upon infection (Kawaguchi et al., 2015, Vale-Costa et al., 2016) and in recruitment of *bona fide* Rab11 effectors, as well as the demonstration that Rab11 enlarged puncta were composed of clustered vesicles (Vale-Costa et al., 2016, Vale-Costa and Amorim, 2016a), containing the a pool of the eight vRNPs (Chou et al., 2013, Lakdawala et al., 2014). Whether vesicular clustering serves a function has not been determined. One appealing hypothesis is that these sites might serve to concentrate vRNPs and promote viral genome assembly. Such hypothesis contrasts other recently proposed models suggesting that genome assembly occurs gradually as ERC vesicles collide on route to the plasma membrane, with the sequential formation of vRNP sub-bundles (with less than eight vRNPs) as reviewed in (Lakdawala et al., 2016). The latter model is supported by an increase in co-localisation of the eight segments found in the Rab11 enlarged structures. Approaches able to resolve whether in clustered vesicles (or Rab11 enlarged structures), the eight segments are found in a complex are necessary to validate one of the models.

IAV modulation of the recycling pathway (Rab11 vesicles) and, in particular, competition between vRNPs and FIPs for Rab11 binding, raised the important question of which host factors, with special attention to molecular motors, were involved in carrying vRNP laden-Rab11 vesicles to the cell periphery (Amorim et al., 2011, Eisfeld et al., 2011, Avilov et al., 2012, Momose et al., 2011). Here we have identified the first motor able to do so. Lack of KIF13A was found to reduce viral titers (Fig 1A), without affecting initial stages of viral infection (Fig 1C,D) or the delivery of virion-forming viral proteins (HA and M2) (Fig 2F) to sites of viral assembly, but impacting on vRNP localization. In the context of overexpression, KIF13A biased the distribution of vRNPs and Rab11 towards the periphery in three different conditions: normal infection (Fig 3, S2, S3, S4), upon nucleozin-treatment (Fig 5, S3, S4) or when Rab11 was artificially tagged to the mitochondria (Fig6, S5, S6). Immunoprecipitation experiments of KIF13A-WT, selectively retrieved Rab11a and Rab11b, but at low levels, which might justify the failure to show vRNP associated to the complex (Fig 4). This association between Rab11 and KIF13A was further corroborated by the nucleozin and mitoRab11a/b strategies that placed all the components in close proximity at the plasma membrane (Fig 5, 6, S2-6). Together these results support the model of Fig 7, in which, conversely to what was observed for FIPs (and presumably the molecular motors these attract), KIF13A binding to Rab11 vesicles is not disrupted by infection and facilitates vRNP transport to the periphery.

The accumulating data regarding alterations in the Rab11 pathway has led to the proposal that, in IAV infection, Rab11 might not be the final factor delivering vRNPs to the surface, handing vRNPs to an additional host protein(s) prior to reaching the membrane (Eisfeld et al., 2015, Vale-Costa et al., 2016, Vale-Costa and Amorim, 2016a). In agreement, a very recent paper provides evidence of a step in the cytoplasmic transport of influenza vRNPs that is independent of Rab11a (Nturibi et al., 2017). Our results show KIF13A-WT accumulating at the plasma membrane (Figs 3, 5, 6, S2-S6) juxtaposed to vRNPs and Rab11, supporting that KIF13A operates in a Rab11 dependent manner. However, the way-station hypothesis might not

be discarded, as vRNPs might be transferred from Rab11 to other cell factor(s) and slide to the cell surface by the action of molecular motors distinct from KIF13A.

It has been shown that impairment of Rab11 vesicular flow leads to clustering of vesicles (Vale-Costa et al., 2016), but the step(s) affected have not been fully understood. Here we focused on vesicular transport on microtubules without investigating other steps required for vesicular flow (biogenesis, attachment and fusion) that also lack characterization. It is clear that in IAV infection, KIF13A does not prevent vesicular clustering late in infection, although it contributes to deliver vRNP-laden Rab11 vesicles to the surface. Whether KIF13A contributes to vesicular clustering requires further investigation. One attractive hypothesis is that at late stages of infection the virus reduces the levels of KIF13A (Fig1B), thus aggravating the impairment in vesicular transport. Other mechanisms might contribute to halt the Rab11 pathway during IAV infection. Alterations in the cytoskeletal structure have been reported to create obstacles to vesicular transport, leading to pausing and movement inhibition (Gramlich et al., 2017, Verdeny-Vilanova et al., 2017). IAV has been shown to alter the structure of microtubules, and of their associated proteins and enzymes, resulting for example in enhanced microtubule acetylation, a modification shown to affect microtubule-based movement (Badding and Dean, 2013). However, these alterations in vRNP transport have not been analysed (Husain and Harrod, 2011). Another parameter worth investigating is how the loading of heavy and large vRNPs influences vesicular transport (Verdeny-Vilanova et al., 2017). Seminal studies imaged fully assembled IAV genomes budding at the plasma membrane (Fournier et al., 2012, Sugita et al., 2013). However, the precise cellular location where genome assembly takes place remains unclear. Recent manuscripts suggested that genome assembly involves formation of vRNP sub-bundles (Chou et al., 2013, Lakdawala et al., 2014). Formation of sub-bundles could lead, or at least contribute, to a halt in vesicular movement resulting in clustering of Rab11 vesicles. Whether clustering of Rab11 vesicles triggers genome assembly or results from partial genome assembly (creating an environment that could facilitate its completion) is still unclear (Vale-Costa et al., 2016, Vale-

Costa and Amorim, 2016a). Intriguingly, studies employing high resolution electron microscopy found no clear evidence of supramolecular complexes in the areas of clustered vesicles (Vale-Costa et al., 2016), although it is very likely that the resolution required for such claim has not been attained. All these studies highlight the fact that the assembly of IAV genome is far from understood. Fascinating outstanding questions that await clarification include: do vRNPs reach the budding sites at the plasma membrane as a sort of supramolecular complex (sub-bundle or complete genome)?; Does vesicular clustering contribute to viral assembly?; What are the molecular mechanisms leading to vesicular clustering?; Is Rab11 the final carrier of vRNP-containing vesicles to the plasma membrane?; and finally, what other means does the virus explore to transport vRNPs (and other viral proteins) to assembly sites?

MATERIALS AND METHODS:

Cells, viruses, plaque assays, infections and drugs:

Human epithelial embryonic kidney (HEK293T) (gift from Dr Colin Adrain, IGC, Portugal), cervical HeLa and alveolar basal cells (A549), and Madin-Darby canine kidney cells (MDCK) were cultured as before (Amorim et al., 2011). Cell lines were a kind gift of Prof Paul Digard, Roslin Institute, UK. All cells are regularly tested for mycoplasma contamination. Reverse-genetics derived A/Puerto Rico/8/34 (PR8; H1N1) was used as a model virus (de Wit et al., 2004) and titrated according to reference (Matrosovich et al., 2006). Statistical analysis of data was done using non-parametric Kolmogorov-Smirnov tests. Additional statistical analyses included a two-way ANOVA test (to include time), followed by Turkey's or Sidak's multiple comparison test (*$p<0.05$, **$p<0.01$, ***$p<0.001$, ns non-significant). Virus infections were performed at a multiplicity of infection (MOI) of 3 (normally as in (Amorim et al., 2011) to 10 (for the mitoRab11 experiment as in (Vale-Costa et al., 2016)). After 30 min, cells were overlaid with DMEM containing 0.14% bovine-serum-albumin. The drug nucleozin (Kao et al., 2010) (Prof. Richard Kao, University of Hong Kong, China) dissolved in DMSO, was used at a final concentration of 2 μM. Reverse genetic plasmids were contributed by Dr Ron Fouchier, Erasmus MC, Netherlands.

Plasmids produced during this study:

Plasmids encoding GFP-tagged KIF13A-WT and GFP-KIF13A-ST were sub-cloned into pEGFP-C2 using SacI and SalI restriction sites subsequently from being amplified using plasmids described in (Delevoye et al., 2014). KIF13A-WT and ST were amplified from pKIF13A-YFP (Graça Raposo). Plasmid encoding cherry-Rab11bWT was produced by PCR-amplification of cDNA from HeLa cells and cloning into EcoRI–BamHI in pcherry-C2 (Clontech). MitoCherry-Rab11b constitutively active (CA) plasmid was produced from cherry-Rab11b. Constitutively

active mutation (Q70L) was introduced by site-directed mutagenesis and fused to the first 105 base pairs of the Tom20 MTS cloned upstream of Cherry–Rab11bCA using NheI–AgeI sites.

The following primers were used:

KIF13A-WT Rv: tcgaGAGCTCAATGTCGGATACCAAGGTAAAAG;

KIF13A-ST Rv: tcgaGAGCTCAAGGATTGTGAACCATGCTG;

KIF13A-WT and ST Fw: tcgaGTCGACTCATTGACAGCACAGAAC;

Rab11b Rv: TGCGGATCCTCACAGGTTCTGGCAGCA;

Rab11b Fw: ATGCGAATTCATGGGGACCCGGGAC;

mitoRab11b Rv: ATGCGGATCCTCACAGGTTCTGGCAGCA;

mitoRab11b Fw: ATGCGAATTCATGGGGACCCGGGAC;

CA mutation Rv: GGTAGCGCTCC**A**GGCCAGCGGTG;

CA mutation Fw: CACCGCTGGCC**T**GGAGCGCTACC;

Tom 20 Rv: ATGCACCGGTTTGAAGTTGGGGTCACTTCG;

Tom 20 Fw: ATGCGCTAGCATGGTGGGTCGGAACAGC.

Transfections of plasmids and siRNA:

Cells (HEK293T or HeLas), 70% confluent in 10-cm dishes were transfected with 250 ng of indicated plasmids using Lipofectamine 2000 (Life Technologies) and Opti-MEM (Life Technologies), according to manufacturer's instructions. 24h post-transfection cells were infected or mock infected at indicated MOI. siRNA transfection of the KIF13A (CTGGCGGGTAGCGAAAGAGTA, S103019800) and negative control (NT, 1022076) RNA duplexes (QIAGEN) was performed in HEK293T and A549 cells grown to approximately 50% confluency the day before transfection. Cells were transfected in 6-well plates (100pmol/well) using DharmaFECT (Dharmacon). When needed 36h later, cells were transfected as above. The mitoRab11a/b experiments was done as in (Vale-Costa et al., 2016), except that plasmids

transfected along with mitoRab11 or mitocherry included GFP, or GFP-KIF13A-WT or GFP-KIF13A-ST.

Real-time reverse-transcription PCR

Extraction of RNA from samples in NZYol (NZYtech, MB18501) was made using the Direct-zol RNA minipreps (Zymo Research, R2052). Reverse transcription was performed using the transcriptor first strand cDNA kit (Roche, 04896866001). Real-time RT-PCR to detect GAPDH and KIF13A was prepared in 384-well, white, thin wall plates (Biorad, HSP3805) using SYBR Green Supermix (Biorad, 172-5124), 10%(v/v) of cDNA and 0.4μM of each primer (KIF13A Fw: GAAGGGAATCAAACGGTCCT; KIF13A Rv: AAACCACTTCTTGACCAGCG; GAPDH Fw: CTCTGCTCCTCCTGTTCGAC; GAPDH Rv: ACCAAATCCGTTGACTCCGAC).

The reaction was performed on a CFX 384 Touch Real-Time PCR Detection System machine (Biorad), using the following PCR conditions: Cycle 1 (1 repeat): 95ºC for 2 minutes; Cycle 2 (40 repeats): 95ºC for 5 seconds and 60ºC for 30 seconds; Cycle 3: 95°C for 5 seconds and melt curve 65ºC to 95ºC (increment 0.05ºC each 5 seconds). Data was analysed using the CFX manager software (Biorad).

Confocal Microscopy

Immunofluorescence assays were performed as in (Simpson-Holley et al., 2002). Antibodies used: rabbit polyclonal against Rab11a (1:100; Life Technologies, 715300); mouse monoclonal against NP (1:1000; Abcam, 20343). Secondary antibodies were all from the Alexa Fluor range (1:1000; Life Technologies). Single optical sections were imaged with a Leica SP5 live or inverted confocal microscope and post-processed using ImageJ (National Institutes of Health; NIH) software for analyses: For vesicle-size analysis (area in μm^2), images were converted to 8-bit color and a 'background subtraction' of 20 pixels applied. Subsequently, 'threshold' was adjusted to 14 (lower level) – 255 (upper level), followed by 'analyze particle' function to quantify each vesicle inside selected cells. Frequency distributions were calculated and plotted using

intervals of [0-0.15], [0.15-0.30] and above 0.30 μm^2; to calculate Pearson correlation coefficient, the 'Coloc 2' function was used; to quantify the percentage of NP and Rab11 perinuclear staining, perinuclear region was defined using the nucleus, delineated by DAPI staining that was then enlarged by 2 µm towards the plasma membrane. This 2 µm region was used to measure intensity of NP (and of Rab11) using integrated density that was divided by the integrated density of NP (and Rab11) staining of the entire cytoplasm. Cell membrane was defined using WGA staining; To quantify accumulation at the periphery the cell edge was defined with WGA, decreased by 2 or 3 µm. The intensity of NP (and of Rab11) was measured within this region using integrated density and divided by the integrated density of NP (and Rab11) staining of the entire cytoplasm. All graphs were plotted using GraphPad Prism. Statistical analysis of data was performed using two-way ANOVA test, followed by Turkey's or Sidak's multiple comparison test (*$p<0.05$, **$p<0.01$, ***$p<0.001$, ns non-significant). At least 25 cells were analysed per condition.

Flow Cytometry:

A549 cells were prepared for flow cytometry analysis by detaching from the wells with trypsin, followed by fixation with 4% paraformaldehyde and washing with PBS in between steps. Cell suspensions were then resuspended in FACS buffer (PBS / 4% FBS). Antibodies used for immunofluorescence staining were: rabbit polyclonal against HA (anti-PR8, 1:500, kind gift from Prof Paul Digard) and M2 (1:100, Abcam, 56086). Secondary antibodies were from Alexa range (1:1000; Life Technologies). Analysis of cell populations was performed in a Becton Dickinson (BD, Franklin Lakes, NJ, USA) FACSCalibur equipped with BD CELLQuest and FlowJo (Tree Star Inc., Ashland, OR, USA) softwares.

Pull-down and Western blotting

Pull down of GFP bound KIF13A was performed using the GFP magnetic agarose beads (ChromoTek, gtm-20). HEK293T cells transfected either with GFP or GFP-KIF13A-WT or GFP-KIF13A-ST and with Cherry-Rab11a WT or Cherry-Rab11b WT were infected or mock infected at an MOI of 5 24h post-transfection. At indicated times, cells were lysed in 500 µl of the provided lysis buffer containing 1 mM phenylmethylsulfonyl fluoride and protease inhibitor cocktail (Roche) on ice for 30 min. Clarified samples were incubated overnight at 4°C with 20 µl GFP-Trap®_M beads. Pelleted beads were washed extensively with lysis buffer and bound proteins were eluted by boiling in SDS-PAGE buffer containing 2.5% β-mercaptoethanol.

Western blotting was performed according to standard procedures and imaged using a LI-COR Biosciences Odyssey near-infrared platform, as described previously (Bruce et al., 2009). Antibodies used included mouse monoclonal against Rab11 (1:500; Abcam, 78337) and NA (7D8, 1:100, gift from Susanna Colaco, University of Cambridge); rabbit monoclonal against virus nucleoprotein (1:2000), and polyclonal against PB1, NS1 and HA (all at 1:500) and provided by Prof Paul Digard; goat polyclonal against GFP (1:2000; Sicgen, AB0020) and M1 (1:500, Abcam, 20910); The secondary antibodies used were from IRDye range (1:10,000; LI-COR Biosciences).

FUNDING INFORMATION:

This project and BK are supported by the project grant awarded by the Fundação para a Ciência e a Tecnologia (FCT), Portugal:PTDC/IMI-MIC/1142/2012. MJA is funded by the FCT investigator fellowship IF/00899/2013; MA and SVC by the FCT postdoc fellowships (SFRH/BPD/62982/2009 and SFRH/BPD/94204/2013, respectively); FF by the Instituto and Fundação Calouste Gulbenkian, Portugal. GR is supported by Fondation pour la Recherche Médicale (Equipe FRM DEQ20140329491 Team label), CD by the Fondation ARC pour la Recherche sur le Cancer (PJA20161204965), and both by CNRS, INSERM and Institut Curie.

AUTHOR CONTRIBUTIONS

ARN, FF, MA, SVC, BK, CD produced tools, performed experiments, analysed data, prepared figures and provided input on the manuscript, GR provided reagents and input on the manuscript, MJA designed the experiments, analysed the data and wrote the manuscript.

ACKNOWLEDGEMENTS

The authors acknowledge Prof Paul Digard (Roslin Institute, UK) for providing reagents (antibodies, cell lines, viral strains and plasmids), and Dr Ron Fouchier (Erasmus, Netherlands) for the reverse genetics plasmids.

REFERENCES

AMORIM, M. J., BRUCE, E. A., READ, E. K., FOEGLEIN, A., MAHEN, R., STUART, A. D. & DIGARD, P. 2011. A Rab11- and microtubule-dependent mechanism for cytoplasmic transport of influenza A virus viral RNA. *J Virol,* 85**,** 4143-56.

AMORIM, M. J., KAO, R. Y. & DIGARD, P. 2013. Nucleozin targets cytoplasmic trafficking of viral ribonucleoprotein-rab11 complexes in influenza a virus infection. *J Virol,* 87**,** 4694-703.

ARRANZ, R., COLOMA, R., CHICHON, F. J., CONESA, J. J., CARRASCOSA, J. L., VALPUESTA, J. M., ORTIN, J. & MARTIN-BENITO, J. 2012. The structure of native influenza virion ribonucleoproteins. *Science,* 338**,** 1634-7.

AVALOS, R. T., YU, Z. & NAYAK, D. P. 1997. Association of influenza virus NP and M1 proteins with cellular cytoskeletal elements in influenza virus-infected cells. *J Virol,* 71**,** 2947-58.

AVILOV, S. V., MOISY, D., NAFFAKH, N. & CUSACK, S. 2012. Influenza A virus progeny vRNP trafficking in live infected cells studied with the virus-encoded fluorescently tagged PB2 protein. *Vaccine,* 30**,** 7411-7.

BADDING, M. A. & DEAN, D. A. 2013. Highly acetylated tubulin permits enhanced interactions with and trafficking of plasmids along microtubules. *Gene Ther,* 20**,** 616-24.

BRUCE, E. A., DIGARD, P. & STUART, A. D. 2010. The Rab11 pathway is required for influenza A virus budding and filament formation. *J Virol,* 84**,** 5848-59.

CHEN, B. J., LESER, G. P., JACKSON, D. & LAMB, R. A. 2008. The influenza virus M2 protein cytoplasmic tail interacts with the M1 protein and influences virus assembly at the site of virus budding. *J Virol,* 82**,** 10059-70.

CHOU, Y. Y., HEATON, N. S., GAO, Q., PALESE, P., SINGER, R. H. & LIONNET, T. 2013. Colocalization of different influenza viral RNA segments in the cytoplasm before viral budding as shown by single-molecule sensitivity FISH analysis. *PLoS Pathog,* 9**,** e1003358.

DE WIT, E., SPRONKEN, M. I., BESTEBROER, T. M., RIMMELZWAAN, G. F., OSTERHAUS, A. D. & FOUCHIER, R. A. 2004. Efficient generation and growth of influenza virus A/PR/8/34 from eight cDNA fragments. *Virus Res,* 103**,** 155-61.

DELEVOYE, C., HURBAIN, I., TENZA, D., SIBARITA, J. B., UZAN-GAFSOU, S., OHNO, H., GEERTS, W. J., VERKLEIJ, A. J., SALAMERO, J., MARKS, M. S. & RAPOSO, G. 2009. AP-1 and KIF13A coordinate endosomal sorting and positioning during melanosome biogenesis. *J Cell Biol,* 187**,** 247-64.

DELEVOYE, C., MISEREY-LENKEI, S., MONTAGNAC, G., GILLES-MARSENS, F., PAUL-GILLOTEAUX, P., GIORDANO, F., WAHARTE, F., MARKS, M. S., GOUD, B. & RAPOSO, G. 2014. Recycling Endosome Tubule Morphogenesis from Sorting Endosomes Requires the Kinesin Motor KIF13A. *Cell Rep,* 6**,** 445-54.

DIGARD, P., ELTON, D., BISHOP, K., MEDCALF, E., WEEDS, A. & POPE, B. 1999. Modulation of nuclear localization of the influenza virus nucleoprotein through interaction with actin filaments. *J Virol,* 73**,** 2222-31.

DOMS, R. W., LAMB, R. A., ROSE, J. K. & HELENIUS, A. 1993. Folding and assembly of viral membrane proteins. *Virology,* 193**,** 545-62.

EISFELD, A. J., KAWAKAMI, E., WATANABE, T., NEUMANN, G. & KAWAOKA, Y. 2011. RAB11A is essential for transport of the influenza virus genome to the plasma membrane. *J Virol,* 85**,** 6117-26.

EISFELD, A. J., NEUMANN, G. & KAWAOKA, Y. 2015. At the centre: influenza A virus ribonucleoproteins. *Nat Rev Microbiol,* 13**,** 28-41.

ELTON, D., SIMPSON-HOLLEY, M., ARCHER, K., MEDCALF, L., HALLAM, R., MCCAULEY, J. & DIGARD, P. 2001. Interaction of the influenza virus nucleoprotein with the cellular CRM1-mediated nuclear export pathway. *J Virol,* 75**,** 408-19.

FAN, G. H., LAPIERRE, L. A., GOLDENRING, J. R., SAI, J. & RICHMOND, A. 2004. Rab11-family interacting protein 2 and myosin Vb are required for CXCR2 recycling and receptor-mediated chemotaxis. *Mol Biol Cell,* 15**,** 2456-69.

FOURNIER, E., MOULES, V., ESSERE, B., PAILLART, J. C., SIRBAT, J. D., ISEL, C., CAVALIER, A., ROLLAND, J. P., THOMAS, D., LINA, B. & MARQUET, R. 2012.

A supramolecular assembly formed by influenza A virus genomic RNA segments. *Nucleic Acids Res,* 40**,** 2197-209.

GERBER, M., ISEL, C., MOULES, V. & MARQUET, R. 2014. Selective packaging of the influenza A genome and consequences for genetic reassortment. *Trends Microbiol,* 22**,** 446-55.

GIESE, S., BOLTE, H. & SCHWEMMLE, M. 2016. The Feat of Packaging Eight Unique Genome Segments. *Viruses,* 8.

GRAMLICH, M. W., CONWAY, L., LIANG, W. H., LABASTIDE, J. A., KING, S. J., XU, J. & ROSS, J. L. 2017. Single Molecule Investigation of Kinesin-1 Motility Using Engineered Microtubule Defects. *Sci Rep,* 7**,** 44290.

HORGAN, C. P. & MCCAFFREY, M. W. 2009. The dynamic Rab11-FIPs. *Biochem Soc Trans,* 37**,** 1032-6.

HUSAIN, M. & HARROD, K. S. 2011. Enhanced acetylation of alpha-tubulin in influenza A virus infected epithelial cells. *FEBS Lett,* 585**,** 128-32.

HUTCHINSON, E. C., CHARLES, P. D., HESTER, S. S., THOMAS, B., TRUDGIAN, D., MARTINEZ-ALONSO, M. & FODOR, E. 2014. Conserved and host-specific features of influenza virion architecture. *Nat Commun,* 5**,** 4816.

HUTCHINSON, E. C., VON KIRCHBACH, J. C., GOG, J. R. & DIGARD, P. 2010. Genome packaging in influenza A virus. *J Gen Virol,* 91**,** 313-28.

KAO, R. Y., YANG, D., LAU, L. S., TSUI, W. H., HU, L., DAI, J., CHAN, M. P., CHAN, C. M., WANG, P., ZHENG, B. J., SUN, J., HUANG, J. D., MADAR, J., CHEN, G., CHEN, H., GUAN, Y. & YUEN, K. Y. 2010. Identification of influenza A nucleoprotein as an antiviral target. *Nat Biotechnol,* 28**,** 600-5.

KAWAGUCHI, A., HIROHAMA, M., HARADA, Y., OSARI, S. & NAGATA, K. 2015. Influenza Virus Induces Cholesterol-Enriched Endocytic Recycling Compartments for Budozone Formation via Cell Cycle-Independent Centrosome Maturation. *PLoS Pathog,* 11**,** e1005284.

LAKDAWALA, S. S., FODOR, E. & SUBBARAO, K. 2016. Moving On Out: Transport and Packaging of Influenza Viral RNA into Virions. *Annu Rev Virol,* 3**,** 411-427.

LAKDAWALA, S. S., WU, Y., WAWRZUSIN, P., KABAT, J., BROADBENT, A. J., LAMIRANDE, E. W., FODOR, E., ALTAN-BONNET, N., SHROFF, H. &

SUBBARAO, K. 2014. Influenza a virus assembly intermediates fuse in the cytoplasm. *PLoS Pathog,* 10**,** e1003971.

LAPIERRE, L. A., KUMAR, R., HALES, C. M., NAVARRE, J., BHARTUR, S. G., BURNETTE, J. O., PROVANCE, D. W., JR., MERCER, J. A., BAHLER, M. & GOLDENRING, J. R. 2001. Myosin vb is associated with plasma membrane recycling systems. *Mol Biol Cell,* 12**,** 1843-57.

MA, K., ROY, A. M. & WHITTAKER, G. R. 2001. Nuclear export of influenza virus ribonucleoproteins: identification of an export intermediate at the nuclear periphery. *Virology,* 282**,** 215-20.

MATROSOVICH, M., MATROSOVICH, T., GARTEN, W. & KLENK, H. D. 2006. New low-viscosity overlay medium for viral plaque assays. *Virol J,* 3**,** 63.

MOMOSE, F., KIKUCHI, Y., KOMASE, K. & MORIKAWA, Y. 2007. Visualization of microtubule-mediated transport of influenza viral progeny ribonucleoprotein. *Microbes Infect,* 9**,** 1422-33.

MOMOSE, F., SEKIMOTO, T., OHKURA, T., JO, S., KAWAGUCHI, A., NAGATA, K. & MORIKAWA, Y. 2011. Apical Transport of Influenza A Virus Ribonucleoprotein Requires Rab11-positive Recycling Endosome. *PLoS One,* 6**,** e21123.

NAKAGAWA, T., SETOU, M., SEOG, D., OGASAWARA, K., DOHMAE, N., TAKIO, K. & HIROKAWA, N. 2000. A novel motor, KIF13A, transports mannose-6-phosphate receptor to plasma membrane through direct interaction with AP-1 complex. *Cell,* 103**,** 569-81.

NODA, T. & KAWAOKA, Y. 2010. Structure of influenza virus ribonucleoprotein complexes and their packaging into virions. *Rev Med Virol,* 20**,** 380-91.

NOTON, S. L., MEDCALF, E., FISHER, D., MULLIN, A. E., ELTON, D. & DIGARD, P. 2007. Identification of the domains of the influenza A virus M1 matrix protein required for NP binding, oligomerization and incorporation into virions. *J Gen Virol,* 88**,** 2280-90.

NTURIBI, E., BHAGWAT, A. R., COBURN, S., MYERBURG, M. M. & LAKDAWALA, S. S. 2017. Intracellular Colocalization of Influenza Viral RNA and Rab11A is Dependent upon Microtubule Filaments. *J Virol*.

PEREZ BAY, A. E., SCHREINER, R., MAZZONI, F., CARVAJAL-GONZALEZ, J. M., GRAVOTTA, D., PERRET, E., LEHMANN MANTARAS, G., ZHU, Y. S. & RODRIGUEZ-BOULAN, E. J. 2013. The kinesin KIF16B mediates apical transcytosis of transferrin receptor in AP-1B-deficient epithelia. *EMBO J,* 32**,** 2125-39.

PFLUG, A., GUILLIGAY, D., REICH, S. & CUSACK, S. 2014. Structure of influenza A polymerase bound to the viral RNA promoter. *Nature,* 516**,** 355-60.

PROVANCE, D. W., JR., ADDISON, E. J., WOOD, P. R., CHEN, D. Z., SILAN, C. M. & MERCER, J. A. 2008. Myosin-Vb functions as a dynamic tether for peripheral endocytic compartments during transferrin trafficking. *BMC Cell Biol,* 9**,** 44.

ROBERTS, P. C. & COMPANS, R. W. 1998. Host cell dependence of viral morphology. *Proc Natl Acad Sci U S A,* 95**,** 5746-51.

ROLAND, J. T., BRYANT, D. M., DATTA, A., ITZEN, A., MOSTOV, K. E. & GOLDENRING, J. R. 2011. Rab GTPase-Myo5B complexes control membrane recycling and epithelial polarization. *Proc Natl Acad Sci U S A,* 108**,** 2789-94.

SCHONTEICH, E., WILSON, G. M., BURDEN, J., HOPKINS, C. R., ANDERSON, K., GOLDENRING, J. R. & PREKERIS, R. 2008. The Rip11/Rab11-FIP5 and kinesin II complex regulates endocytic protein recycling. *J Cell Sci,* 121**,** 3824-33.

SHAW, M. L., STONE, K. L., COLANGELO, C. M., GULCICEK, E. E. & PALESE, P. 2008. Cellular proteins in influenza virus particles. *PLoS Pathog,* 4**,** e1000085.

SIMPSON-HOLLEY, M., ELLIS, D., FISHER, D., ELTON, D., MCCAULEY, J. & DIGARD, P. 2002. A functional link between the actin cytoskeleton and lipid rafts during budding of filamentous influenza virions. *Virology,* 301**,** 212-25.

SUGITA, Y., SAGARA, H., NODA, T. & KAWAOKA, Y. 2013. Configuration of viral ribonucleoprotein complexes within the influenza A virion. *J Virol,* 87**,** 12879-84.

SUN, E., HE, J. & ZHUANG, X. 2013. Dissecting the role of COPI complexes in influenza virus infection. *J Virol,* 87**,** 2673-85.

VALE-COSTA, S., ALENQUER, M., SOUSA, A. L., KELLEN, B., RAMALHO, J., TRANFIELD, E. M. & AMORIM, M. J. 2016. Influenza A virus ribonucleoproteins modulate host recycling by competing with Rab11 effectors. *J Cell Sci,* 129**,** 1697-710.

VALE-COSTA, S. & AMORIM, M. J. 2016a. Clustering of Rab11 vesicles in influenza A virus infected cells creates hotspots containing the eight viral ribonucleoproteins. *Small GTPases*, 0.

VALE-COSTA, S. & AMORIM, M. J. 2016b. Recycling Endosomes and Viral Infection. *Viruses,* 8.

VERDENY-VILANOVA, I., WEHNEKAMP, F., MOHAN, N., SANDOVAL ALVAREZ, A., BORBELY, J. S., OTTERSTROM, J. J., LAMB, D. C. & LAKADAMYALI, M. 2017. 3D motion of vesicles along microtubules helps them to circumvent obstacles in cells. *J Cell Sci,* 130, 1904-1916.

WELZ, T., WELLBOURNE-WOOD, J. & KERKHOFF, E. 2014. Orchestration of cell surface proteins by Rab11. *Trends in cell biology,* 24, 407-15.

XIONG, B., BAYAT, V., JAISWAL, M., ZHANG, K., SANDOVAL, H., CHARNG, W. L., LI, T., DAVID, G., DURAINE, L., LIN, Y. Q., NEELY, G. G., YAMAMOTO, S. & BELLEN, H. J. 2012. Crag is a GEF for Rab11 required for rhodopsin trafficking and maintenance of adult photoreceptor cells. *PLoS Biol,* 10, e1001438.

YAMAYOSHI, S., WATANABE, M., GOTO, H. & KAWAOKA, Y. 2015. Identification of A Novel Viral Protein Expressed from the PB2 Segment of Influenza A Virus. *J Virol*.

Figures

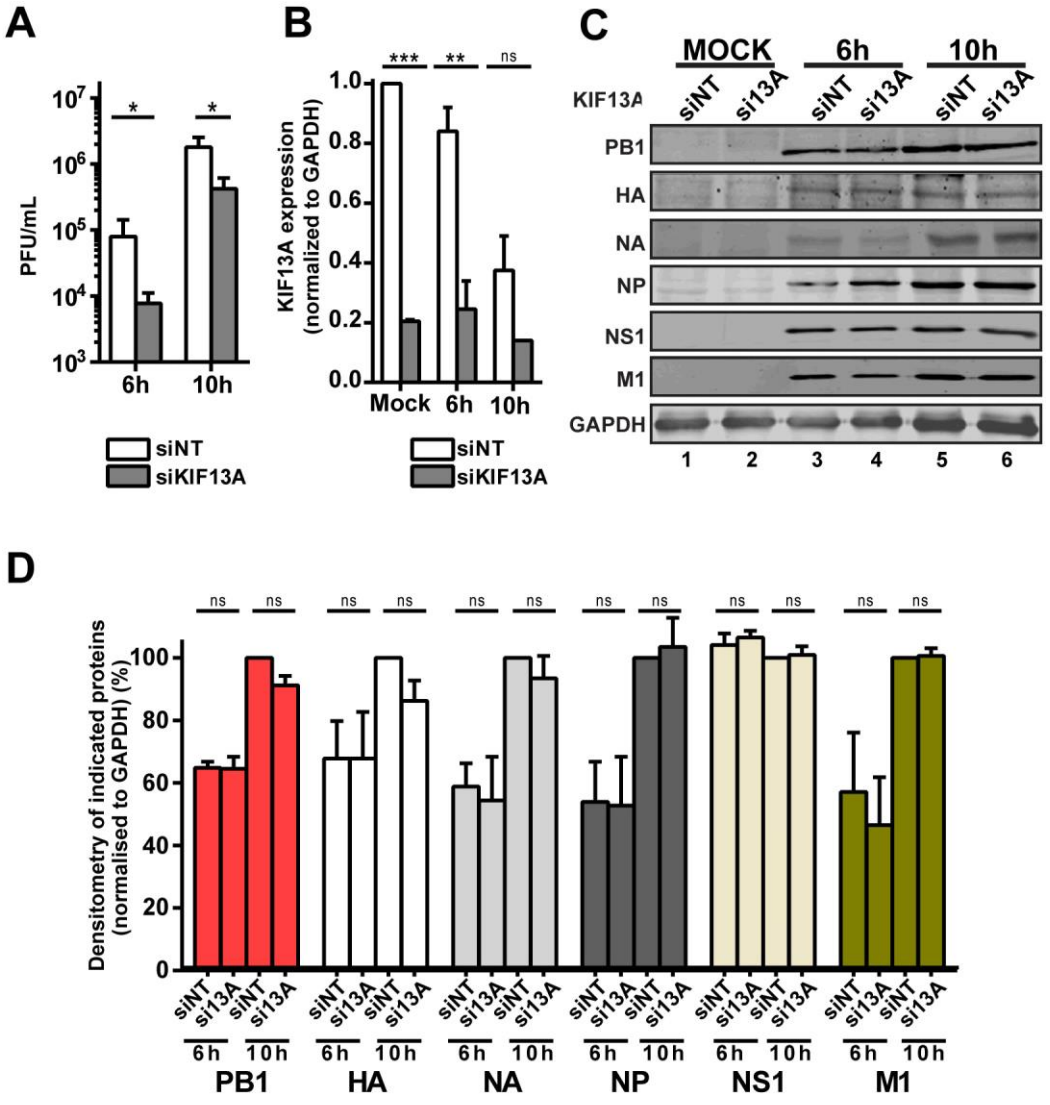

Fig 1. KIF13A depletion leads to a drop in virus titres, without affecting viral protein expression.

A549 cells were treated with non-targeting or KIF13A specific siRNAs and infected or mock-infected with PR8 at a multiplicity of infection (MOI) of 3. At the indicated time points **A.** supernatants were collected and viral production evaluated by plaque assays, or cells were

collected. Statistical analysis of data was performed using non-parametric Kolmogorov-Smirnov test, unpaired (*p<0.05) and **B.** KIF13A expression was evaluated at the level of transcription by RT-qPCR in relation to GAPDH; and **C.** of viral protein expression of PB1, HA, NA, NP, NS1, M1 and the control GAPDH by western blotting. Expression of viral proteins was quantified and normalized to GAPDH and presented as percentage of each protein in the non-targeting siRNA condition at 10h **D.** Data is shown as means±SEM from four independent experiments and statistical significance is indicated as **p <0.01, ***p <0.001 by non-parametric two-way ANOVA tests followed by Tukey multiple comparison test.

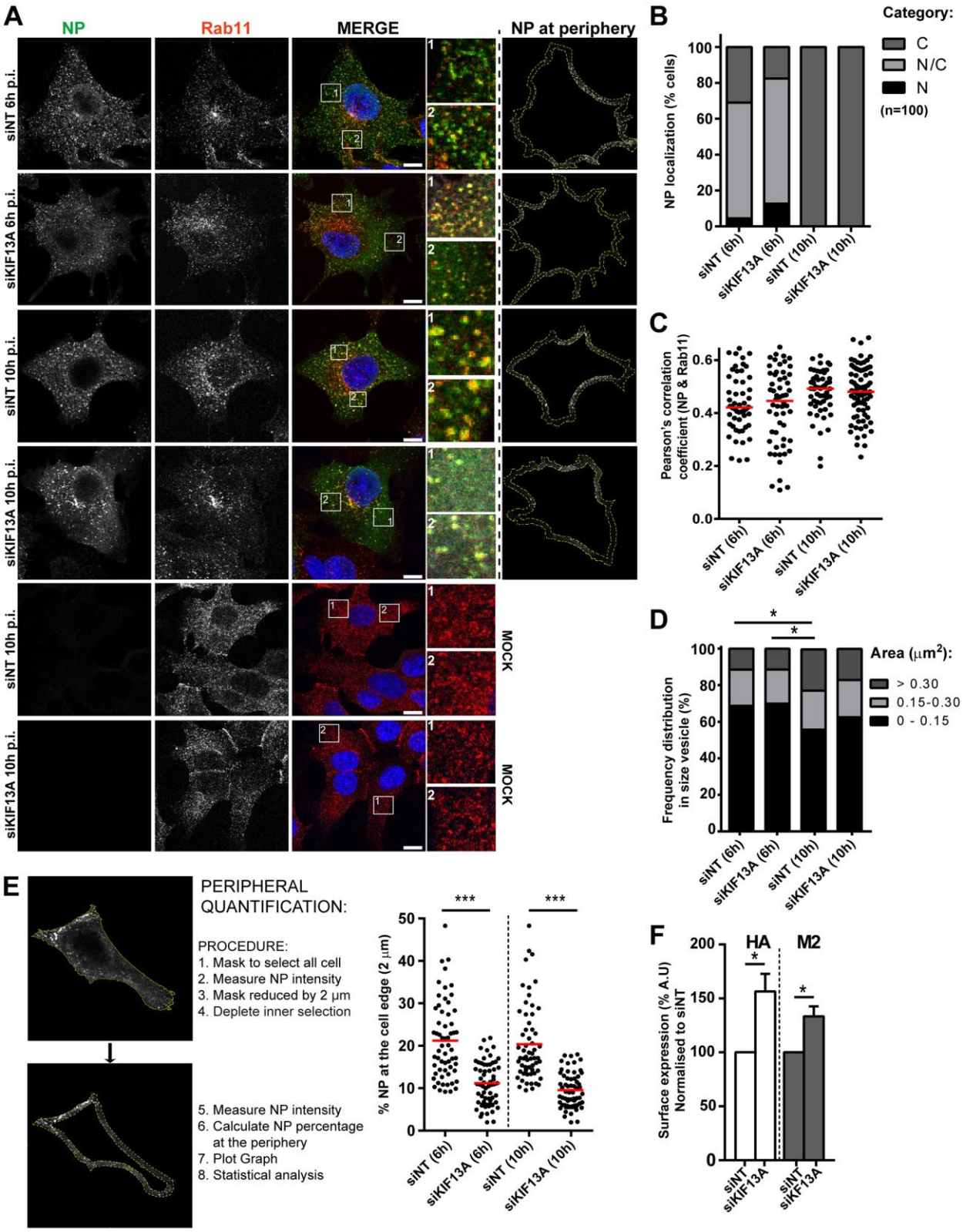

Fig 2. KIF13A depletion reduces the levels of vRNPs close to the plasma membrane, but not that of the viral transmembrane HA and M2 proteins.

A549 cells were treated with non-targeting or KIF13A specific siRNAs and infected or mock-infected with PR8 at a MOI of 3. At indicated time points, cells were fixed and processed for immunofluorescence staining of endogenous Rab11 (red) and viral NP protein (as proxy for vRNPs and in green) **A.** Images were acquired at a SP5 confocal microscope (scale bar=10 μm). The panels on the right show NP staining (black & white) within 2 μm from the cell edge that was obtained as demonstrated in **E.**; and **B.** 50 cells per condition were evaluated and quantified for nuclear, nuclear-cytoplasmic or cytoplasmic localisation of NP. Statistical analysis was performed using two-way ANOVA followed by Sidak's multiple comparison test. **C.** Pearson correlation for NP and Rab11 was calculated at least on 50 cells per condition in three independent replicates using the Fiji plugin co-localization threshold. Statistical analysis was performed using one-way ANOVA followed by Kruskal-Wallis multiple comparison test and were considered significant at *p<0.05. **D.** The frequency distribution of three size categories in the areas (in μm^2) of Rab11-vesicles (small, medium and large) was calculated based on NP staining and plotted. Statistical analysis of data was performed using an ANOVA test and were considered significant at *p<0.05. 30 cells were analyzed per condition in four independent experiments. Statistical analysis herein indicated compares only the larger interval of all samples for the four replicates. **E.** The percentage of NP at the edge of the cell was quantified by calculating the ratio in NP intensity within 2 μm from the plasma membrane in relation to NP intensity of the whole cell. The value of 30 cells in three replicates was plotted and analysed statistically using one-way ANOVA followed by Tukey's multiple comparisons test and were considered significant at ***p<0.001. **F.** A549 cells were treated with non-targeting or KIF13A specific siRNAs and infected or mock-infected with PR8 at a MOI of 3. At 10h p.i., the surface

levels of viral HA and M2 proteins were analysed by flow cytometry and plotted as percentage in arbitrary units. Statistical analysis was done using one-way ANOVA followed by Sidak method to compare samples for three replicates and were considered significant at *$p<0.05$.

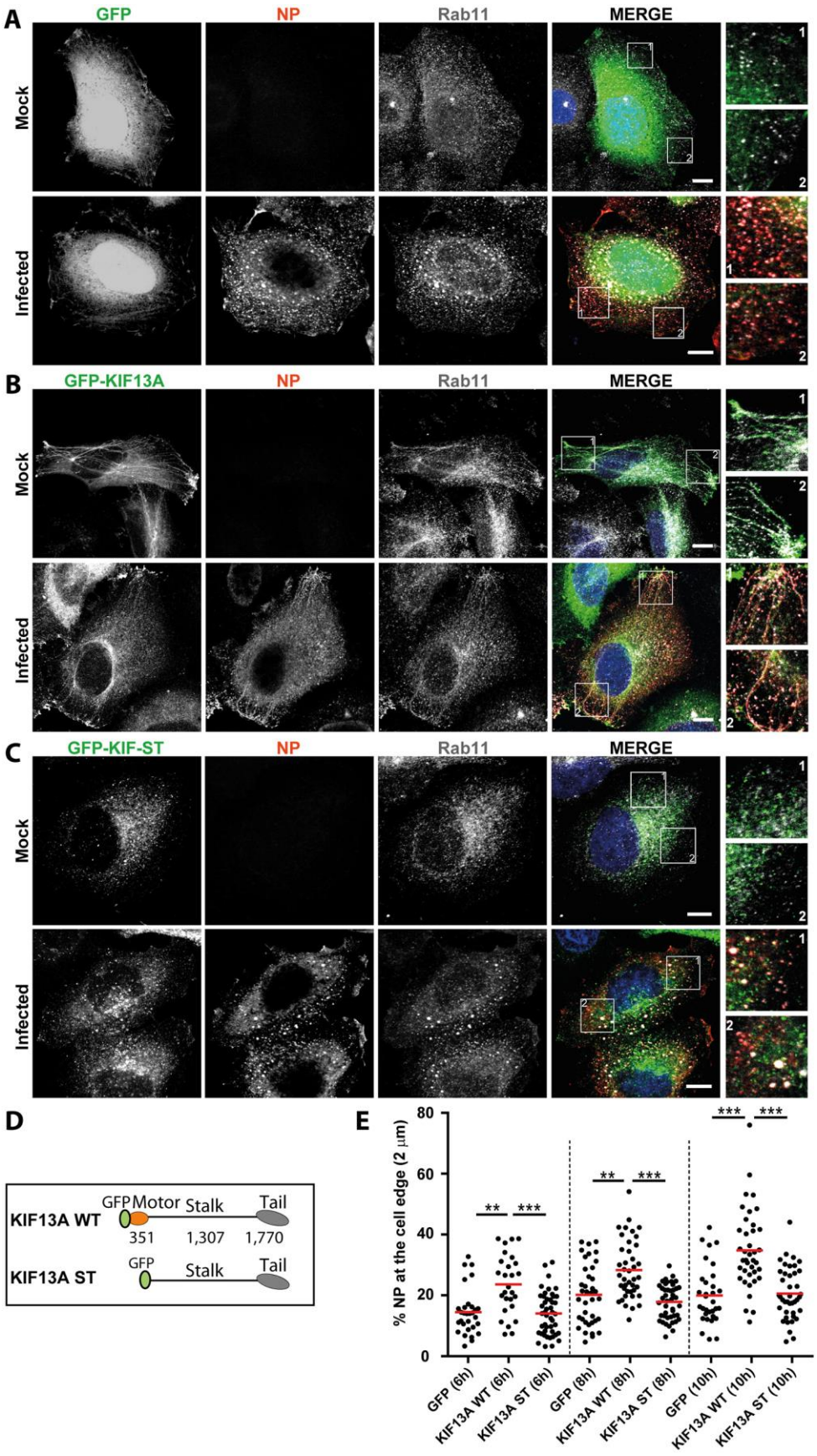

Fig 3. KIF13A overexpression biases NP distribution to the cell edge and requires KIF13A binding to microtubules.

HeLa cells were transfected with **A.** GFP **B.** GFP-KIF13A-WT or **C.** GFP-KIF13A-ST. These KIF13A forms are depicted in **D. A-C**, 24h post-transfection cells were infected (or mock-infected) with PR8 at a MOI=3 and fixed at 8h p.i. and stained for NP (red), endogenous Rab11 (grey) and counterstained with DAPI (scale bar=10 μm). **E.** The percentage of NP at the edge of the cell was quantified by calculating the ratio in NP intensity within 2 μm from the plasma membrane in relation to NP intensity of the whole cell. The value of 25 cells from three replicates was plotted and analysed statistically using one-way ANOVA followed by Tukey's multiple comparisons, and were considered significant at **$p<0.01$ and ***$p<0.001$.

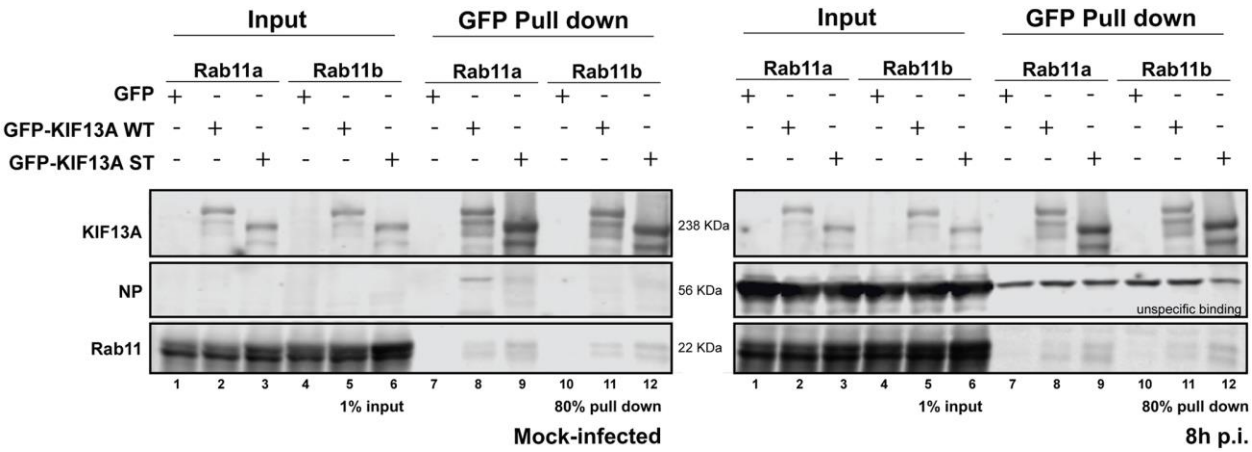

Fig 4. KIF13A-WT and -ST pull down Rab11a and Rab11b.

293T cells were transfected individually with GFP, or GFP-KIF13A-WT or GFP-KIF13A-ST in combination with either cherry-Rab11a-WT or Cherry-Rab11b-WT. 24h post-transfection cells were infected (or mock-infected) with PR8 at a MOI=3 and at 8h p.i., GFP was immunoprecipitated using GFP-TRAP. Input (1% of total) and pulled down complexes (80% of total) were separated by electrophoresis and KIF13A, NP and Rab11 analysed by western blot. The western blot is representative of three independent experiments.

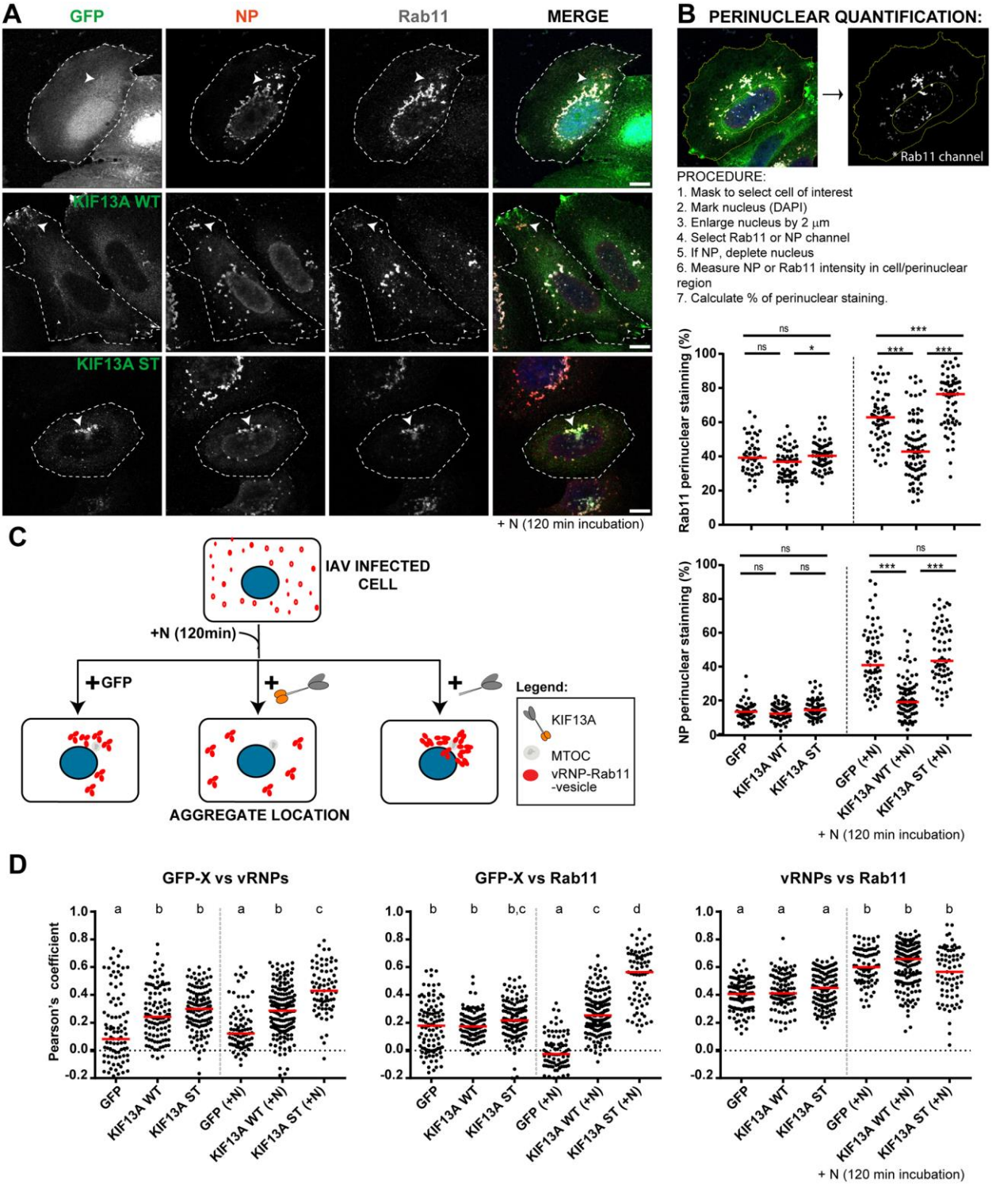

Fig 5. Nucleozin-induced collapse of vRNP aggregates close to the nucleus is less pronounced in the presence of KIF13A.

HeLa cells were transfected individually with GFP, or GFP-KIF13A-WT or GFP-KIF13A-ST. 24 h post-transfection cells were infected (or mock-infected) with PR8 at a MOI=3 and at 8h p.i. 2 μM nucleozin was added and incubated for 2h. Cells were then fixed and stained for NP (red) and Rab11 (grey) and counterstained with DAPI **A**. Representative images of three independent experiments (scale bar=10 μm). **B.** The percentage of vRNPs (by measuring NP) and Rab11 close to the nucleus (within 2 μm) relative to that found in the whole cell was quantified in 60 cells and plotted. The value of 20 cells in three replicates was plotted and analysed statistically using two-way ANOVA followed by Tukey's multiple comparisons test and were considered significant at ***p<0.001. **C.** Model to explain how KIF13-WT counteracts the action of nucleozin. It was reported that nucleozin has affinity for two binding sites on NP and hence crosslinks colliding vRNP-laden Rab11 vesicles leading to large agglomerates that collapse near the nucleus. In our experimental set up, addition of GFP did not affect the collapse of vRNPs/Rab11, but that of KIF13A-WT resulted in decreased perinuclear levels of vRNPs, suggesting that KIF13A counteracts nucleozin action by pulling vRNPs away from the minus end. KIF13A action required binding to microtubules, as the mutant KIF13A-ST was unable to counteract nucleozin action. **D.** Pearson correlation value between GFP-x (x=-,KIF13A-WT, KIF13A-ST) and NP or Rab11, as well as between NP and Rab11 in the presence and absence of nucleozin was calculated at least on 50 cells per condition in three independent replicates using the Fiji plugin co-localization threshold. Statistical analysis was performed using one-way ANOVA followed by Kruskal-Wallis multiple comparison test. Letters (a, b and c) are coding for comparisons that are significant at least at **p<0.01.

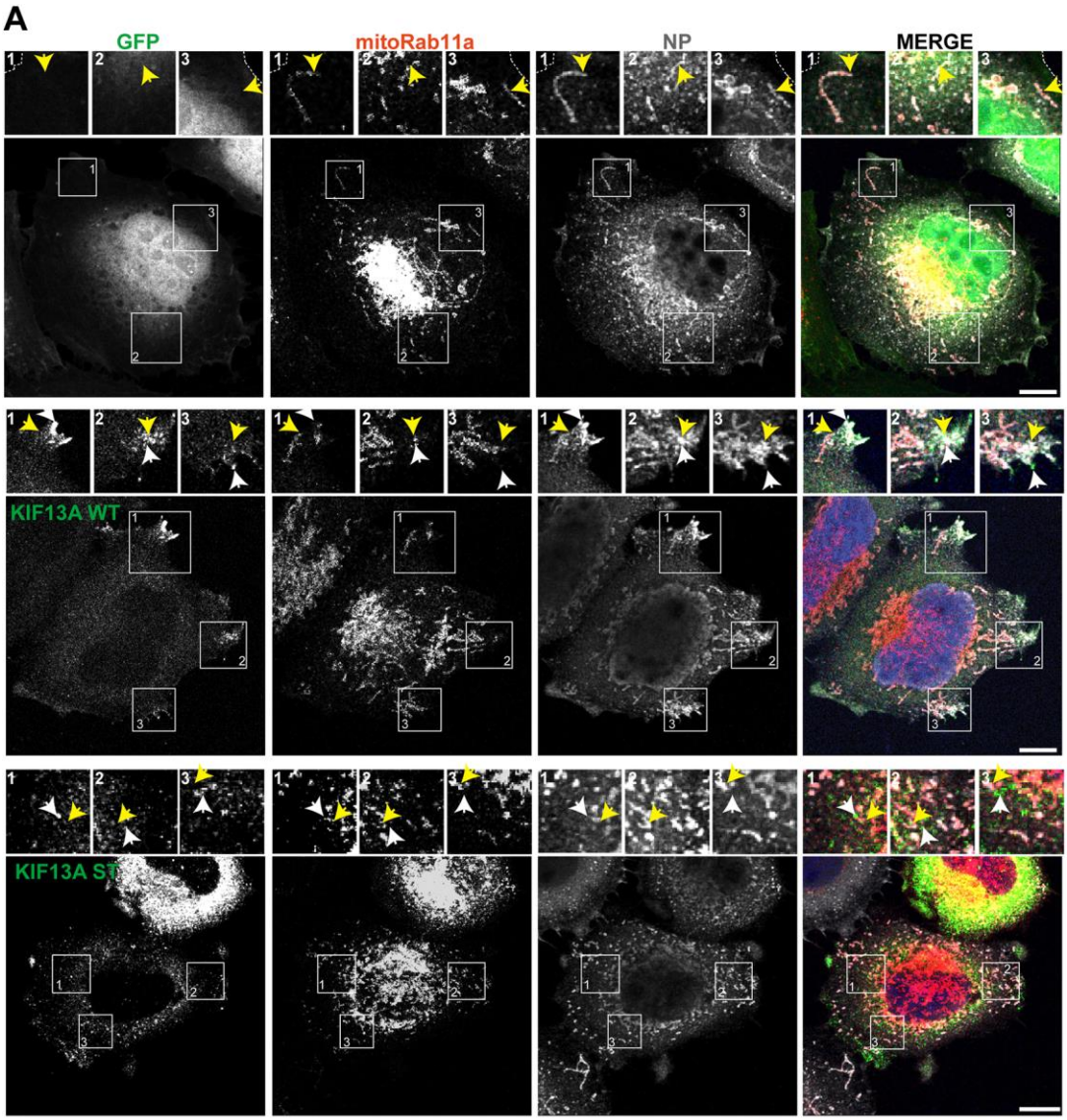

Fig 6. KIF13A-WT biases the localisation of mitochondria to the periphery when artificially expressing Rab11a or Rab11b.

HeLa cells were transfected individually with GFP, or GFP-KIF13A-WT or GFP-KIF13A-ST and mitocherry or mitoRab11a or mitoRab11b. 24h post-transfection cells were infected (or mock-infected) with PR8 at a MOI=10. At 14h p.i, cells were fixed and stained for NP (grey) and Rab11 (red) and counterstained with DAPI **A**. Representative images of three independent experiments (scale bar=10 μm). **B.** Diagram explaining the strategy used to artificially target cherry, Rab11a or Rab11b to the mitochondria. **C.** Pearson correlation value between NP and mitocherry/mitoRab11 were calculated for 20 cells per condition from independent replicates using the Fiji plugin co-localization threshold. Statistical analysis was performed using one-way ANOVA followed by Kruskal-Wallis multiple comparison test. **D.** The percentage of NP/mitoRab11a/b at the edge of the cell was quantified by calculating the ratio in NP intensity within 3 μm from the plasma membrane in relation to NP/mitoRab11a/b intensity of the whole cell. The value of at least 20 cells in three replicates was plotted and analysed statistically using one-way ANOVA followed by Sidak's multiple comparisons test and were considered significant at *$p<0.05$, **$p<0.01$ and ***$p<0.001$.

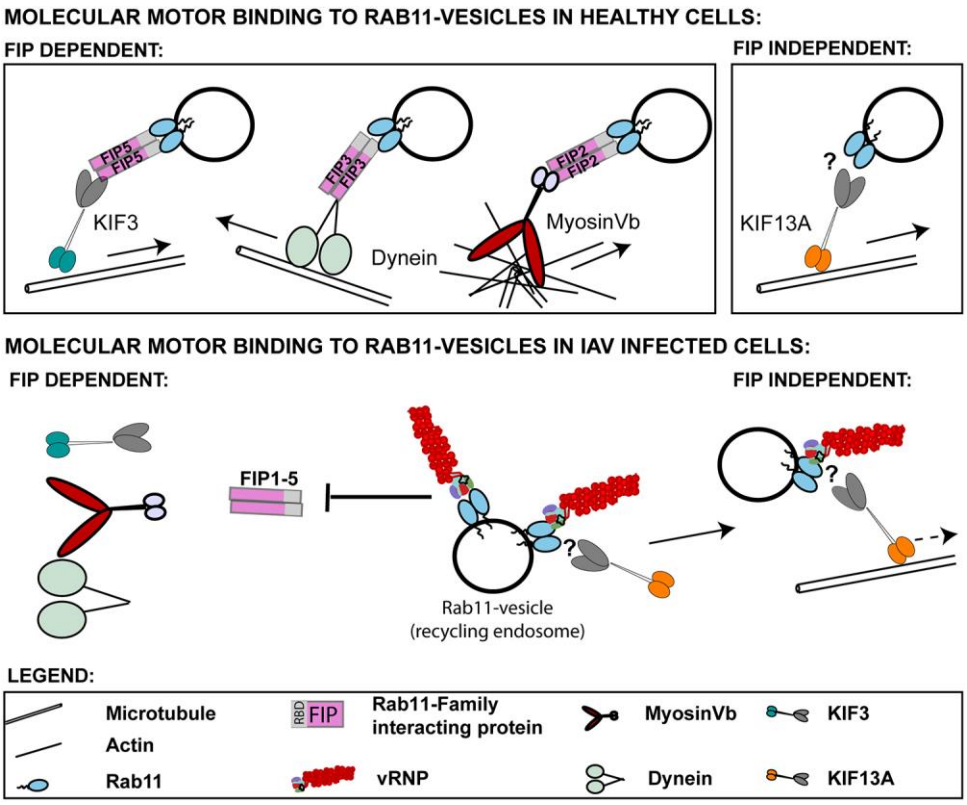

Fig 7. Model for molecular motor recruitment of Rab11-vesicles during IAV infection.

In the healthy cell, GTP bound Rab11 associates with FIPs that are able to recruit members of the three types of molecular motors known: kinesins, dynein and myosin. In addition GTP-Rab11 is also able to attract molecular motors independently of FIPs as is the case of KIF13A. We previously showed that in IAV infected cells, vRNPs outcompete FIPs for Rab11 binding (Vale-Costa et al., 2016). In the present study we report that the molecular motor KIF13A is able to bind and transport vRNP-Rab11 carrying vesicles. At late stages of infection the levels of KIF13A are reduced and might affect transport (hence the dashed line indicating movement). The molecular players mediating the interaction in our system are still unclear.

Supplementary Figures

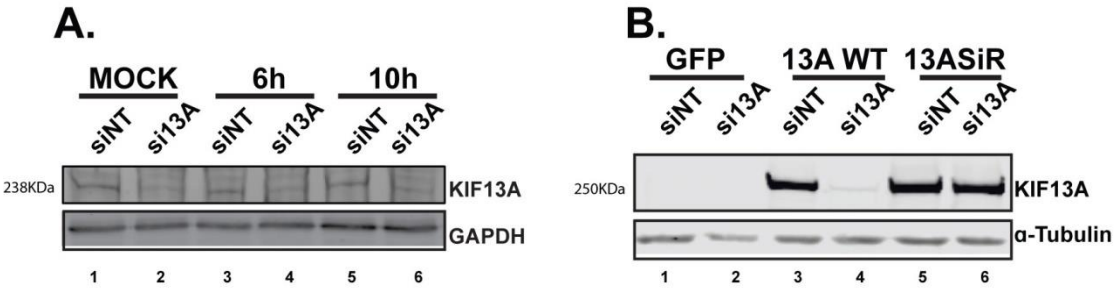

Figure S1 - KIF13A protein levels are efficiently reduced by siRNA treatment.

A. A549 cells were treated with non-targeting or KIF13A specific siRNAs and infected or mock-infected with PR8 at a multiplicity of infection (MOI) of 3. At indicated time points, cells were collected and KIF13A and GAPDH levels analysed by western blot. **B.** HeLa cells were treated with non-targeting or KIF13A specific siRNAs and transfected with GFP or GFP-KIF13A-WT or a GFP-KIF13A-WT mutant that is resistant to the siRNA duplexes used and incubated for 24h**.** The GFP-KIF13A siRNA resistant (siR) mutant was generated based on the GFP-KIF13A WT plasmid, by insertion of two mutations using site-directed mutagenesis (Agilent). The following primers were used: 5′- GTAAGGTCAGCTTGGTAGACCTAGCAGGGAGCGAAAGAGTATCTA -3′ (KIF13A siR Fw); 5′- TAGATACTCTTTCGCTCCCTGCTAGGTCTACCAAGCTGACCTTAC -3’ (KIF13A siR Rv). KIF13A was analysed by western blotting and compared to α-tubulin loading control. Images are representative of at least three independent experiments.

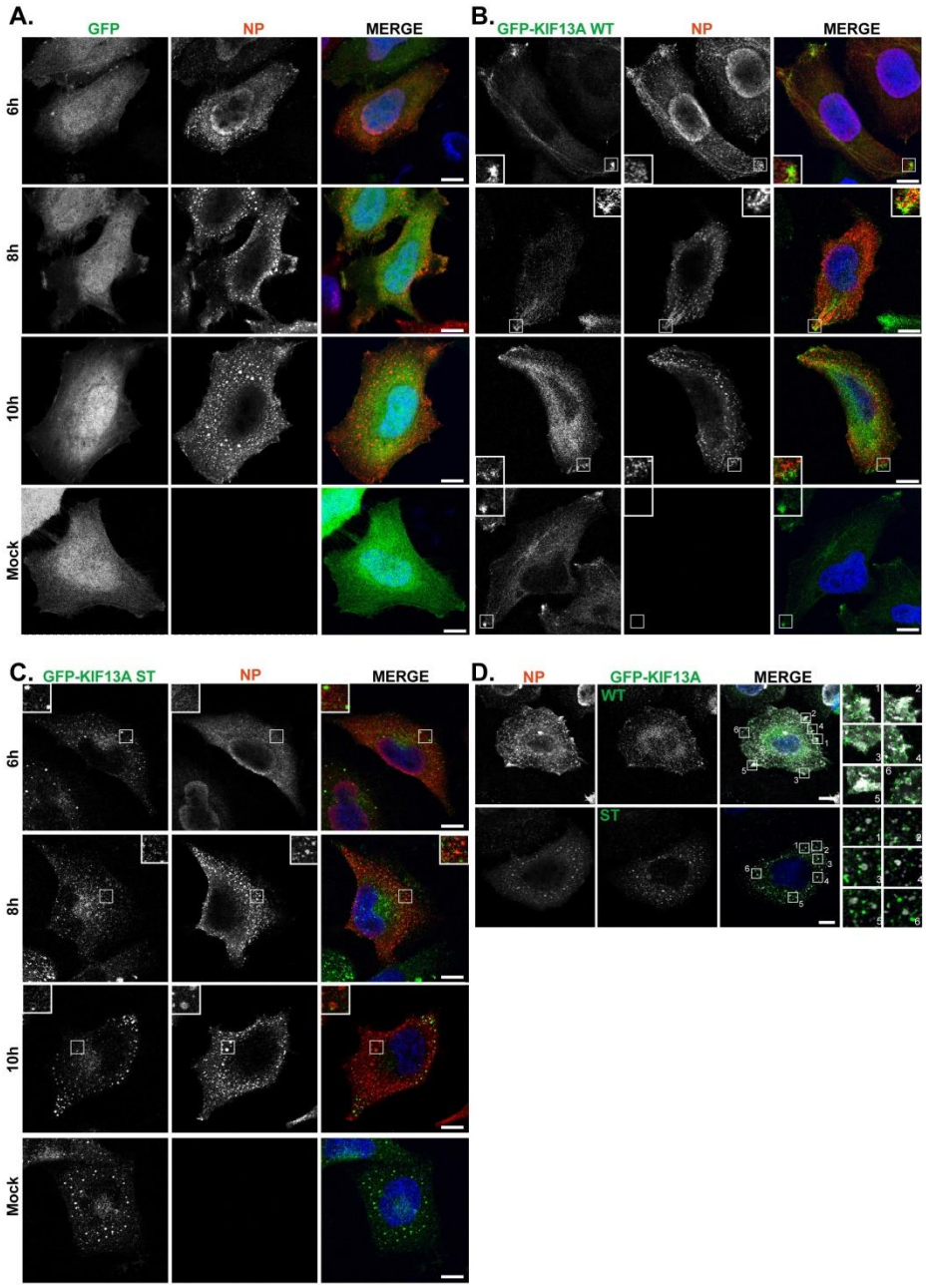

Figure S2. KIF13A overexpression biases NP distribution to the cell edge and requires KIF13A binding to microtubules.

HeLa cells were transfected with **A.** GFP **B.** GFP-KIF13A-WT or **C.** GFP-KIF13A-ST. **A-D**, 24 h post-transfection cells were infected (or mock-infected) with PR8 at a MOI=3 and fixed at the indicated time points and stained for NP (red) and counterstained with DAPI. **D.** Shows several inlets of infected cells at 8h p.i.. Scale bar represents 10 μm. Images are representative of six independent experiments.

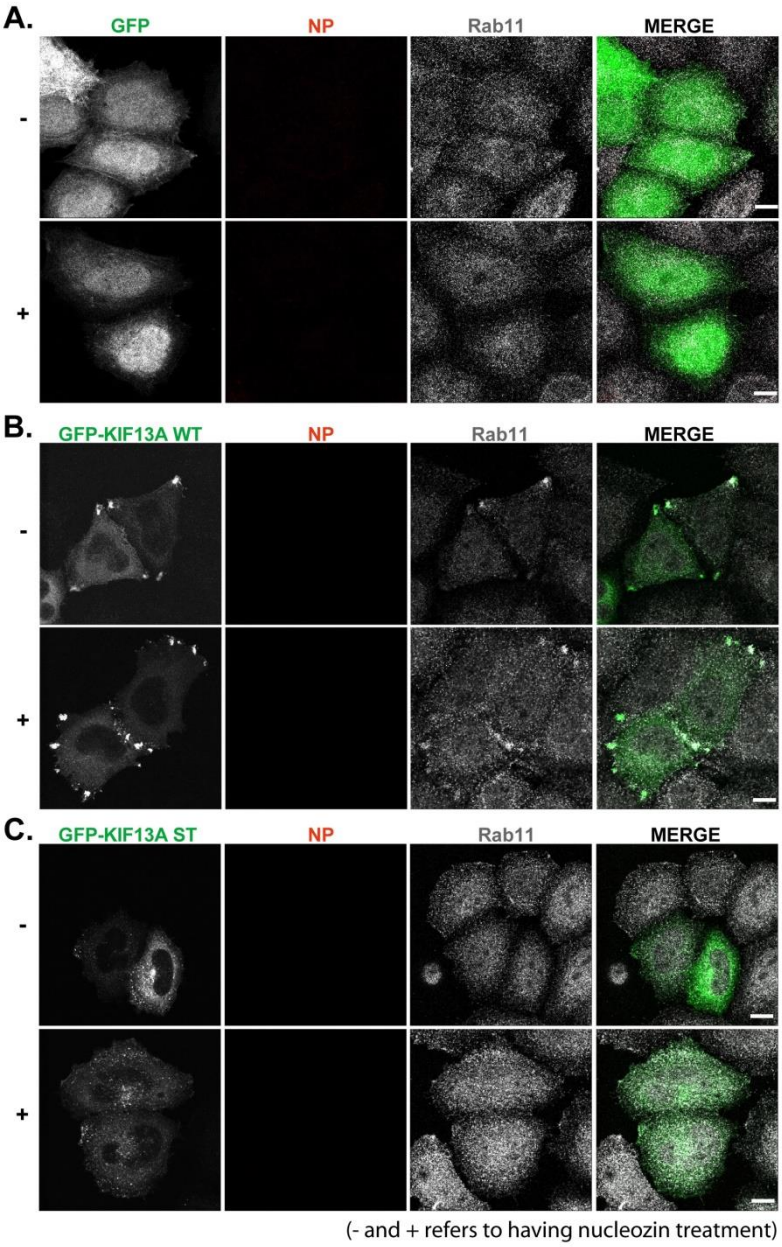

Figure S3 - Nucleozin treatment is not efficient in mock infected cells. HeLa cells were transfected individually with 250 ng of GFP, or GFP-KIF13A WT or GFP-KIF13A ST and incubated for 24 hours before being overlaid with Opti-MEM for 8 h prior to being overlaid with SFM containing (+) or not (-) 2 μM nucleozin for 2 h. Cells were then fixed and stained for NP (Red) and Rab11 (grey). Note that when GFP-KIF13A WT is present, endogenous Rab11 concentrates at the cell periphery, co-localising with KIF13A. Scale bar represents 10 μm. Images are representative of three independent experiments.

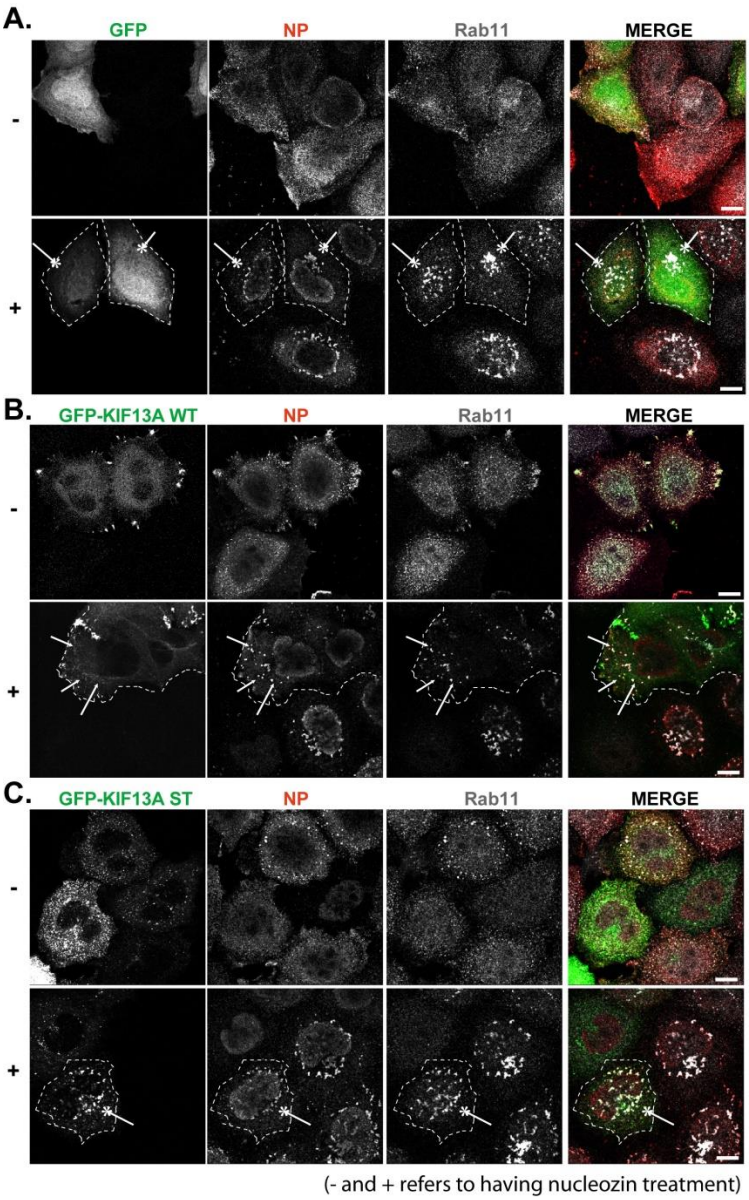

Figure S4 - KIF13A reduces nucleozin-induced perinuclear localization of vRNPs and Rab11 in infected cells. HeLa cells were transfected individually with 250 ng of GFP, or GFP-KIF13A WT or GFP-KIF13A ST and incubated for 24 hours before being infected with PR8 at a MOI of 20. 8 h p.i. cells were treated (+) or not (-) with 2 μM nucleozin for 2 h. Cells were then fixed and stained for NP (Red) and Rab11 (grey). Note that nucleozin treatment induces formation of vRNP (and Rab11) aggregates as described in (Amorim et al., 2013). In the presence of GFP-KIF13A-WT, aggregates do not concentrate so close to the nucleus, as in the presence of GFP or GFP-KIF13A-ST, a form unable to attach to molecular motors. Scale bar represents 10 μm. Images are representative of three independent experiments.

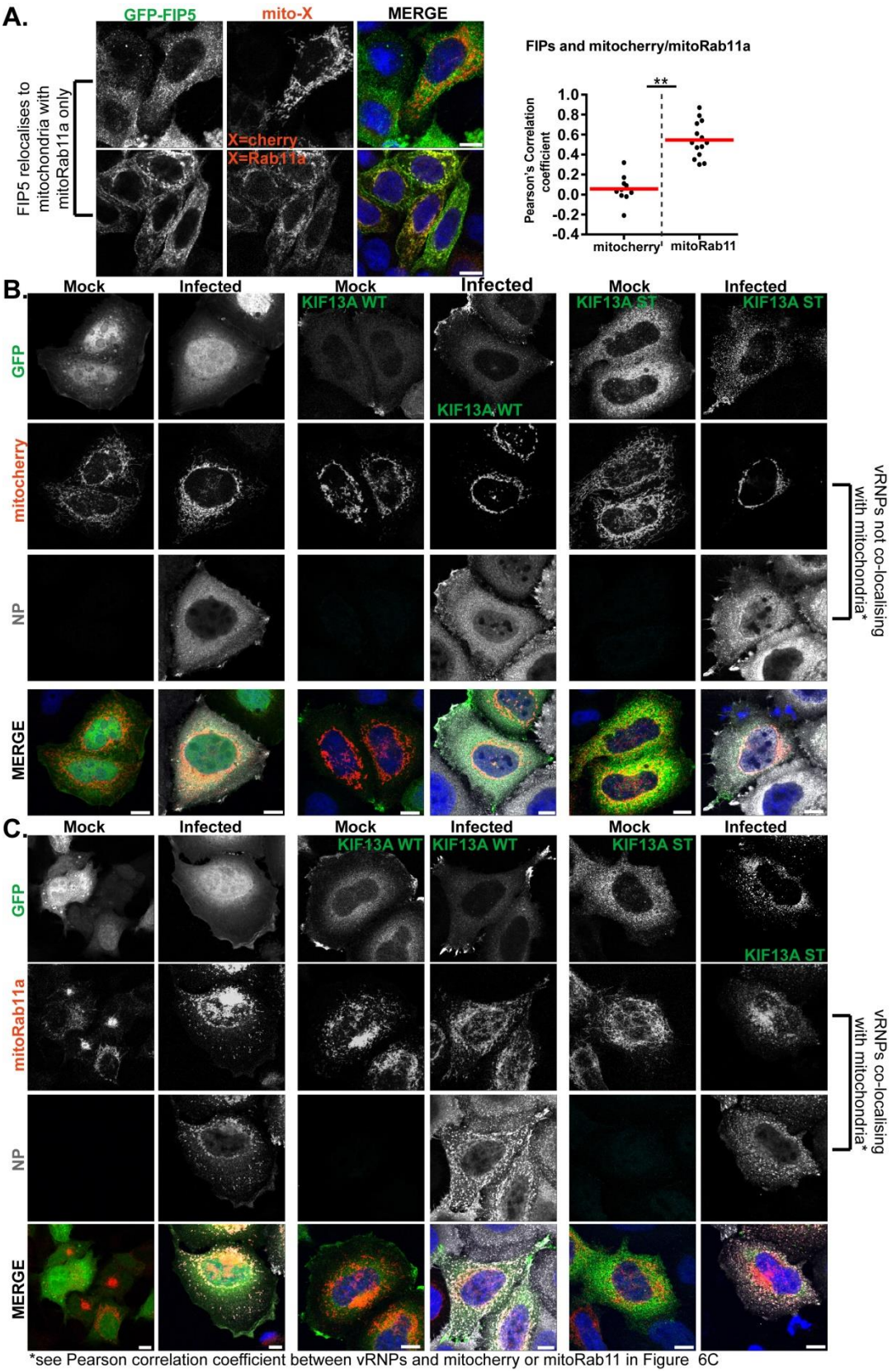
A.
GFP-FIP5
mito-X
MERGE
FIP5 relocalises to mitochondria with mitoRab11a only
X=cherry
X=Rab11a
FIPs and mitocherry/mitoRab11a
Pearson's Correlation coefficient
1.0
0.8
0.6
0.4
0.2
0.0
-0.2
-0.4
**
mitocherry
mitoRab11
B.
Mock
Infected
Mock
KIF13A WT
Infected
KIF13A WT
Mock
KIF13A ST
Infected
KIF13A ST
GFP
mitocherry
NP
MERGE
vRNPs not co-localising with mitochondria*
C.
Mock
Infected
Mock
KIF13A WT
Infected
KIF13A WT
Mock
KIF13A ST
Infected
KIF13A ST
GFP
mitoRab11a
NP
MERGE
vRNPs co-localising with mitochondria*
*see Pearson correlation coefficient between vRNPs and mitocherry or mitoRab11 in Figure 6C

Figure S5 - KIF13A-WT biases mitoRab11a and vRNP to the periphery.

A. HeLa cells were transfected with GFP-FIP5 and mitocherry or mitoRab11aCA and incubated for 14h, before being fixed and processed for imaging. DAPI was included to stain the nucleus. Pearson correlation values between GFP-FIP5 and mito were calculated for 10 cells using the Fiji plugin co-localization threshold. This analysis was meant to corroborate published material (Vale-Costa and Amorim, 2016a). Statistical analysis was performed using one-way ANOVA followed by Kruskal-Wallis multiple comparison test (**p<0.01). **B,C.** HeLa cells were transfected with GFP, GFP-KIF13A-WT or GFP-KIF13A-ST and with mitocherry or mitoRab11aCA and infected (or mock infected) with PR8 at MOI 10. At 14h p.i., cells were fixed and processed for immunofluorescence staining of viral NP (Scale bar = 10 μm). Note that vRNPs relocate to mitochondria exclusively in the presence of mitoRab11a. Images are representative of three independent experiments.

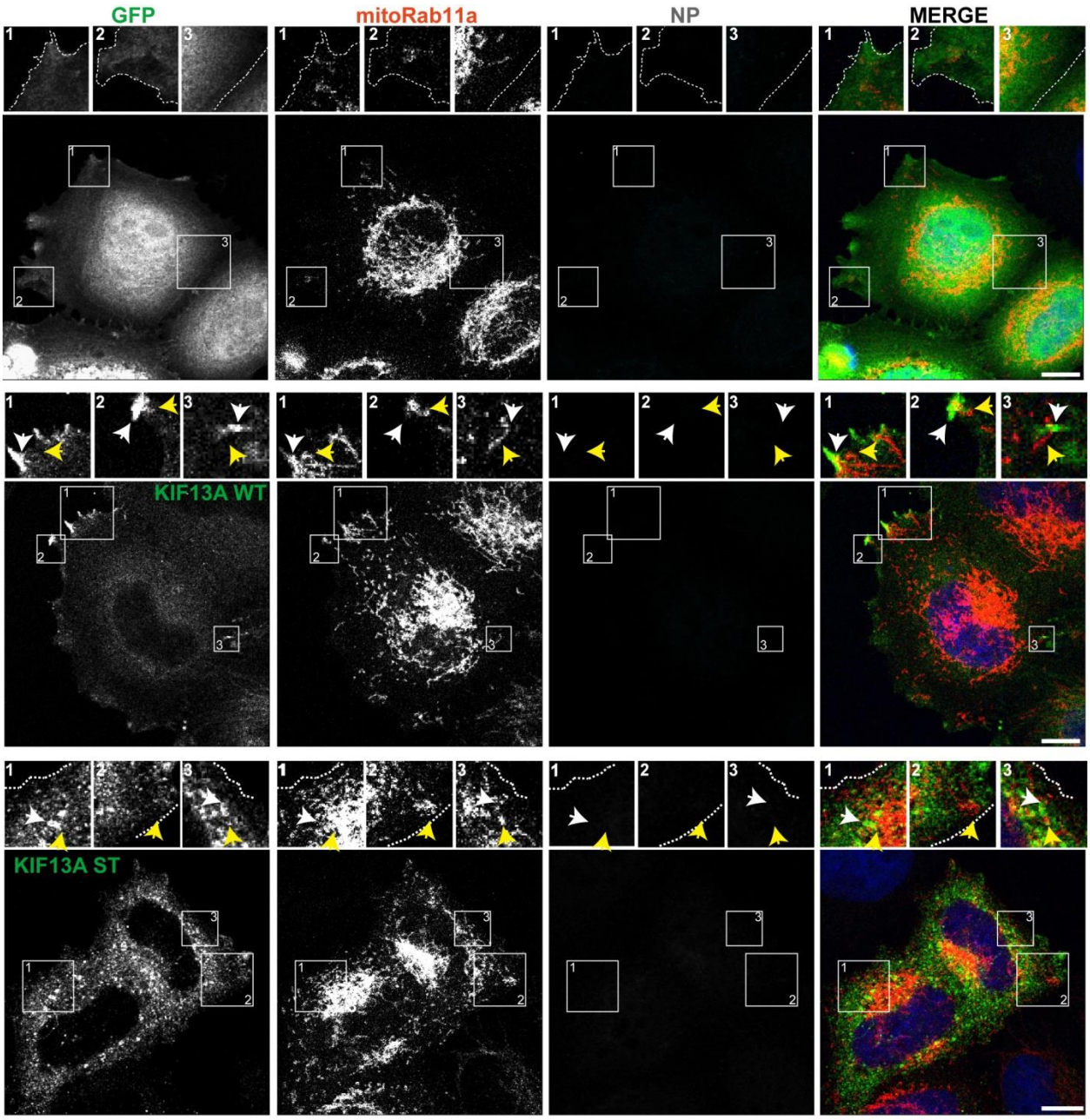

Figure S6 - KIF13A-WT biases mitoRab11a to the periphery in uninfected cells and requires its motor activity. HeLa cells were transfected individually with GFP, or GFP-KIF13A-WT or GFP-KIF13A-ST and mitocherry or mitoRab11a or mitoRab11b for 32h, time at which cells were fixed and stained for NP (red), Rab11 (grey) and counterstained with DAPI (blue) (scale bar=10 μm). Images are representative of three independent experiments.